Supporting information

Synthesis and chiral optical activity of quadruple heterohelicene based on 1,4-dihydropyrrolo[3,2-*b*]pyrrole–picene hybrid

Krzysztof J. Kochanowski, Krzysztof Górski, Damian Kusy, Nicolas Vanthuyne, Alessandro Landi, Francesco Bertocchi, Arkadiusz Ciesielski, Michał K. Cyrański, Guglielmo Monaco*, Francesca Terenziani*, and Daniel T. Gryko*

Table of Contents

1. General remarks

All reagents and solvents were purchased from commercial sources and were used as received unless otherwise noted. For water-sensitive reactions solvents were dried using Solvent Purification System from MBraun (https://www.mbraun.com/us/). Reactions involving moisture and oxygen sensitive compounds were performed under a stream of argon. The reaction progress was monitored by means of thin layer chromatography (TLC), which was performed on aluminum foil plates, covered with Silica gel 60 F254 (Merck). Products purification was done by means of column chromatography with Kieselgel 60 (200-400 mesh, Merck). The identity and purity of prepared compounds were proved by ^{1}H NMR and ^{13}C NMR spectrometry as well as by MS-spectrometry (via EI-MS , ESI-MS or APCI-MS). NMR spectra were measured on Bruker AM 500 MHz, Varian 600 MHz, Varian 500 MHz instruments with TMS as internal standard. Chemical shifts for ^{1}H NMR are expressed in parts per million (ppm) relative to tetramethylsilane (δ 0.00 ppm), $CDCl_3$ (δ 7.26 ppm) CD_2Cl_2 (δ 5.33 ppm). Chemical shifts for ^{13}C NMR are expressed in ppm relative to $CDCl_3$ (δ 77.16 ppm), CD_2Cl_2 (53.84 ppm). Data are reported as follows: chemical shift, multiplicity (s = singlet, bs = broad singlet, d = doublet, dd = doublet of doublets, ddd = doublet of doublet of doublets, t = triplet, td = triplet of doublets, q = quartet, qu = quintet, m = multiplet), coupling constant (Hz), and integration.

2. Experimental section

Picen-13-yl trifluoromethanosulfonate S1

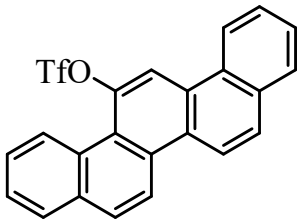

Picen-13-ol as a raw product (synthesized according to Lin[1]) was introduced into a round-bottom flask (1.02 g, 3.47 mmol, 1 equivalent), which was purged with argon. Anhydrous dichloromethane (30 ml), dry triethylamine (0.58 ml, 4.16 mmol, 1.2 equivalents) were added and the mixture was cooled to 0°C. Trifluoromethanesulfonic anhydride (0.64 ml, 3.81 mmol, 1.1 equivalents) was added dropwise, and the mixture was allowed to warm to room temperature. The reaction was terminated after complete conversion of the substrate (after 16 hours), which was confirmed by TLC, by adding water (20 ml), and the layers were separated. The aqueous layer was extracted with dichloromethane (3x20 ml), and the combined organic layers were dried over $MgSO_4$ and evaporated under reduced pressure after removal of the drying agent. The crude product was purified by column chromatography on silica gel (SiO_2, hexane/dichloromethane 1:1). 1.21 g of product was obtained as a beige solid (yield: 82%).

^{1}H NMR (600 MHz, Methylene chloride-d_2) δ 9.24 (d, J = 8.5 Hz, 1H), 8.83 (s, 1H), 8.77 (d, J = 9.2 Hz, 1H), 8.71 (d, J = 9.2 Hz, 2H), 8.69 (d, J = 8.3 Hz, 2H), 8.10 (t, J = 8.5 Hz, 2H), 8.07 (dd, J = 7.7, 1.4 Hz, 1H), 8.05 (dd, J = 7.9, 1.4 Hz, 1H), 7.85 – 7.67 (m, 4H).

^{13}C{^{1}H} NMR (151 MHz, Methylene chloride-d_2) δ 146.5, 133.5, 132.8, 132.3, 130.2, 130.2, 129.5, 129.3, 129.2, 128.7, 128.7, 128.4, 128.2, 128.1, 128.1, 127.9, 127.8, 123.5, 122.3, 121.8, 121.7, 119.3 (q, J = 321.0, CF_3), 116.1.

HRMS (APCI) calculated for $C_{23}H_{14}O_3F_3$: 427.0616, found: 427.0617 $[M+H]^+$.

2-(picen-13-yl)benzaldehyde 1

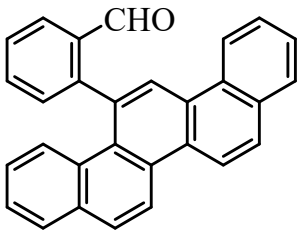

Picen-13-yl triflate (852 mg, 2.0 mmol, 1 equivalent), o-formylphenylboronic acid (449 mg, 3.0 mmol, 1.5 equivalents), $Pd(PPh_3)_4$ (231 mg, 0.2 mmol, 0.1 equivalent), K_3PO_4 (2.12 g, 10.0 mmol, 5 equivalents) and 20 ml of dry toluene under an argon flow. The resulting mixture was degassed three times by vacuum/argon cycles, then placed in an oil bath preheated to 80°C and heated for 19 hours. After this time, it was cooled to room temperature and 10 ml of water was added. The aqueous layer was extracted with dichloromethane (3x40 ml). The combined organic layers were dried over $MgSO_4$, the drying agent was drained off, and the mixture was concentrated under reduced pressure. Cyclohexane was added and the resulting precipitate was filtered off and washed with cyclohexane. The dark green solid obtained was purified by column chromatography on silica gel (SiO_2, hexane/ethyl acetate 4:1). A beige solid was obtained (yield: 60%).

^{1}H NMR (600 MHz, Methylene chloride-d_2) δ 9.72 (s, 1H), 8.91 (d, J = 9.2 Hz, 1H), 8.84 (d, J = 9.2 Hz, 1H), 8.75 (d, J = 7.9 Hz, 1H), 8.72 (s, 1H), 8.14 (dd, J = 7.8, 1.5 Hz, 1H), 8.10 (dd, J = 9.1, 3.4 Hz, 2H), 8.05 (dd, J = 7.4, 1.8 Hz, 1H), 7.98 (dd, J = 8.0, 1.5 Hz, 1H), 7.82 (dt, J = 7.5, 1.5 Hz, 1H), 7.73 – 7.67 (m, 3H), 7.67 – 7.63 (m, 2H), 7.50 (ddd, J = 7.9, 6.8, 1.1 Hz, 1H), 7.16 (ddd, J = 8.6, 6.8, 1.5 Hz, 1H).

^{13}C{^{1}H} NMR (151 MHz, Methylene chloride-d_2) δ 191.6, 149.1, 134.5, 134.1, 133.8, 133.4, 132.1, 131.2, 130.0, 130.0, 128.6, 128.6, 128.5, 128.5, 128.2, 128.2, 128.1, 127.9, 127.8, 127.5, 127.0, 127.0, 126.9, 126.2, 125.5, 123.1, 121.7, 121.5.

HRMS (APCI) calculated for $C_{29}H_{19}O_2$: 383.1436, found: 383.1439 $[M+H]^+$.

1,4-bis(4-octylphenyl)-2,5-bis(2-(picen-13-yl)phenyl)-1,4-dihydropyrrolo[3,2-b]pyrrole 2

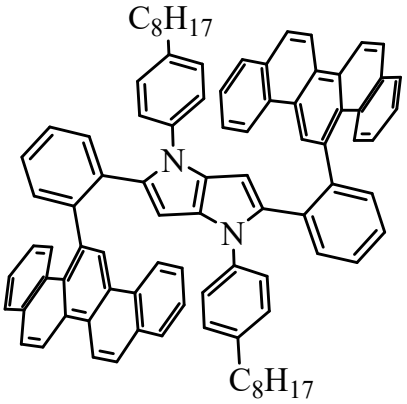

To a 25 ml round-bottom flask equipped with a magnetic stirrer, 208 mg of aldehyde **1** (243 mg, 0.635 mmol, 2 equivalents) was added to a 25 ml round-bottom flask equipped with a magnetic stirrer, dissolved by adding acetic acid (1.5 ml) and toluene (1.5 ml), and then 4-n-octylaniline (130 mg, 0.635 mmol, 2 equivalents) was introduced. The flask was placed in a preheated oil bath at 50°C for 15 minutes. After this time, $Fe(ClO_4)_3 \cdot xH_2O$ (7 mg) and diacetyl (0.027 ml, 0.318 mmol, 1 equivalent) were added. The mixture was further heated at 50°C in an oil bath in an open flask for 16 hours. After cooling the mixture to room temperature, methanol was added. The resulting precipitate was filtered and washed with additional methanol. In order to obtain an analytically pure product, purification by column chromatography (SiO_2, hexane/ethyl acetate 9:1) was used. 280 mg of a yellowish solid was obtained (yield: 74%).

^{1}H NMR (500 MHz, Methylene chroride-d_2) Mixture of atropoisomers (ratio~1:1) δ 8.72 (d, J = 9.2 Hz, 1H), 8.64 (d, J = 9.2 Hz, 1H), 8.47 – 8.33 (m, 3H), 8.22-8.03 (m, 7H), 7.73 (d, J = 8.6 Hz, 1H), 7.70 – 7.64 (m, 2H), 7.64 – 7.52 (m, 3H), 7.52 – 7.35 (m, 10H), 7.33 (d, J = 7.9 Hz, 1H), 7.26 (dd, J = 7.9, 1.5 Hz, 1H), 7.23 – 7.14 (m, 3H), 7.12 – 7.07 (m, 1H), 7.02 (ddd, J = 8.5, 6.9, 1.5 Hz, 1H), 6.90 (ddd, J = 8.5, 6.9, 1.5 Hz, 1H), 6.44 (d, J = 8.0 Hz, 2H), 6.27 (d, J = 7.8 Hz, 2H), 6.02 (d, J = 8.2 Hz, 2H), 5.98 (d, J = 7.9 Hz, 2H), 2.23 – 2.13 (m, 1H), 2.12 – 2.01 (m, 2H), 1.98 – 1.87 (m, 1H), 1.38 – 1.20 (m, 24H), 1.00 – 0.91 (m, 6H).

^{13}C{^{1}H} NMR (126 MHz, Methylene chloride-d_2) δ 138.9, 138.9, 136.8, 136.7, 132.3, 132.2, 131.9, 131.8, 130.6, 130.4, 130.3, 129.1, 129.0, 128.3, 128.2, 128.0, 127.8, 127.7, 127.6, 127.6, 127.5, 127.4, 127.4, 127.4, 127.2, 127.1, 127.1, 126.6, 126.5, 126.5, 126.4, 125.3, 125.3, 124.7, 124.5, 123.5, 123.3, 123.2, 122.7, 122.7, 121.7, 121.7, 121.0, 120.9, 34.8, 34.7, 32.0, 31.9, 31.2, 30.9, 30.8, 29.9, 29.7, 29.5, 29.4, 29.4, 29.3, 29.3, 22.7, 22.7, 13.9, 13.9.

HRMS (APCI) calculated for $C_{90}H_{79}N_2$: 1187.6243, found: 1187.6227 $[M+H]^+$.

3,6-dibromo-1,4-bis(4-octylphenyl)-2,5-bis(2-(picen-13-yl)phenyl)-1,4-dihydropyrrolo[3,2-b]pyrrole 3

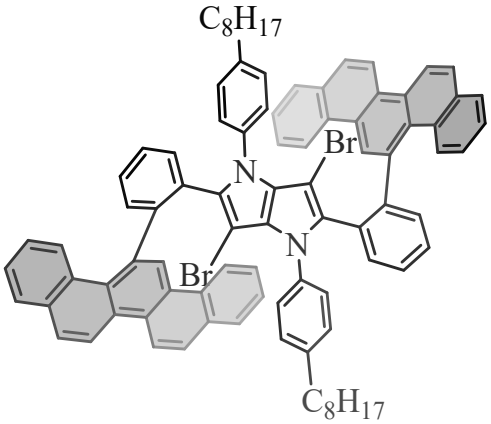

The resulting TAPP **2** (77.5 mg, 0.065 mmol, 1 equivalent) was placed in a 25 ml round-bottom flask and dissolved in 1.5 ml $CHCl_3$, then NBS (29 mg, 0.163 mmol, 2.5 equivalents) was added in a single portion. The mixture was heated in an oil bath for 16 hours at boiling point (65°C). After this time, the chloroform was evaporated and methanol (10 ml) was added. The precipitate was filtered and washed with additional methanol. 84 mg of the desired product was obtained, which was used for the next reaction without further purification (yield: 96%).

HRMS (APCI) calculated for $C_{90}H_{77}N_2Br_2$: 1343.4454, found: 1343.4445 $[M+H]^+$.

11,28-bis(4-octylphenyl)-11,28-dihydrobenzo[g]benzo[6,7]piceno[13',14':4,5]indolo[3,2-b]piceno[13,14-e]indole 4

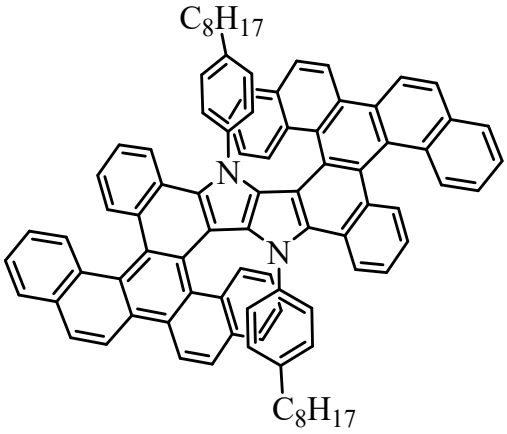

Compound **3** (120 mg, 0.089 mmol, 1 equivalent), Cs_2CO_3 (87.2 mg, 0.268 mmol, 3 equivalents), PPh_3 (11.7 mg, 0.045 mmol, 0.5 equivalent), $Pd(OAc)_2$ (4 mg, 0.018 mmol, 0.2 equivalent) and 8 ml of dry toluene were added under a stream of argon. The Schlenk flask was placed in an oil bath preheated to 120°C. After 16 hours, the mixture was cooled to room temperature, 5 ml of DCM was added, and the mixture was filtered through celite and concentrated. The crude product was purified by column chromatography on

silica gel (SiO_2, hexane -> hexane/ethyl acetate 40:1). 83 mg of yellow solid was obtained (yield: 79%).

HRMS (APCI) calculated for $C_{90}H_{75}N_2$: 1183.5930, found: 1183.5947 $[M+H]^+$.

Meso form of **4**:

^{1}H NMR (600 MHz, Methylene chloride-d_2) δ 8.92 (d, J = 9.2 Hz, 2H), 8.71 (d, J = 8.5 Hz, 2H), 8.66 (d, J = 9.2 Hz, 2H), 8.30 (d, J = 8.5 Hz, 2H), 8.12 (d, J = 8.9 Hz, 2H), 8.04 (t, J = 8.9 Hz, 4H), 7.71 (d, J = 8.9 Hz, 2H), 7.66 (d, J = 7.4 Hz, 2H), 7.56 (t, J = 7.1 Hz, 2H), 7.39 – 7.33 (m, 2H), 7.28 (t, J = 7.1 Hz, 2H), 7.05 (d, J = 8.5 Hz, 2H), 6.97 (ddd, J = 8.2, 6.6, 1.4 Hz, 2H), 6.93 (ddd, J = 8.1, 6.5, 1.4 Hz, 2H), 6.88 (ddd, J = 8.1, 6.5, 1.3 Hz, 2H), 6.65 – 6.61 (m, 4H), 6.55 (dd, J = 7.9, 2.3 Hz, 2H), 6.37 (dd, J = 7.8, 2.0 Hz, 2H), 2.63 – 2.50 (m, 4H), 1.73 – 1.66 (m, 4H), 1.46 – 1.29 (m, 20H), 0.90 (t, J = 6.7 Hz, 6H).

^{13}C{^{1}H} (126 MHz, Methylene chloride-d_2) δ 140.7, 135.9, 133.0, 132.0, 132.0, 131.6, 130.3, 130.1, 130.1, 129.9, 129.2, 128.5, 128.4, 128.1, 128.1, 127.9, 127.2, 127.0, 126.7, 126.6, 126.1, 125.8, 125.8, 125.5, 125.5, 125.3, 125.3, 124.7, 124.7, 124.7, 124.6, 124.0, 122.9, 122.8, 121.7, 121.4, 120.2, 110.9, 35.5, 32.0, 30.8, 29.7, 29.6, 29.4, 22.8, 13.9.

Enantiomeric form of compound **4**:

^{1}H NMR (500 MHz, Methylene chloride-d_2) δ 9.24 (d, J = 6.2 Hz, 1H), 8.76 (d, J = 9.2 Hz, 1H), 8.61 (d, J = 9.2 Hz, 1H), 8.13 (d, J = 8.9 Hz, 1H), 8.10 (d, J = 8.0 Hz, 1H), 8.03 – 7.96 (m, 3H), 7.91 (d, J = 7.8 Hz, 1H), 7.74 – 7.65 (m, 2H), 7.54 (t, J = 7.8 Hz, 1H), 7.38 (t, J = 7.3 Hz, 1H), 7.01 (t, J = 7.8 Hz, 2H), 6.90 (t, J = 7.5 Hz, 1H), 6.64 (d, J = 8.0 Hz, 1H), 6.26 (d, J = 7.7 Hz, 1H), 6.23 (d, J = 8.0 Hz, 1H), 6.18 (d, J = 7.5 Hz, 1H), 2.47 – 2.28 (m, 2H)

^{13}C{^{1}H} NMR (126 MHz, Methylene chloride-d_2) δ 127.3, 121.4, 120.8, 130.1, 128.2, 130.4, 126.5, 127.9, 127.7, 121.8, 126.0, 125.4, 125.8, 124.3, 125.0, 122.3, 127.7, 130.4, 35.4, 31.2, 22.8, 29.4, 32.0, 29.5, 29.7, 13.9.

3. ^{1}H and ^{13}C NMR spectral data

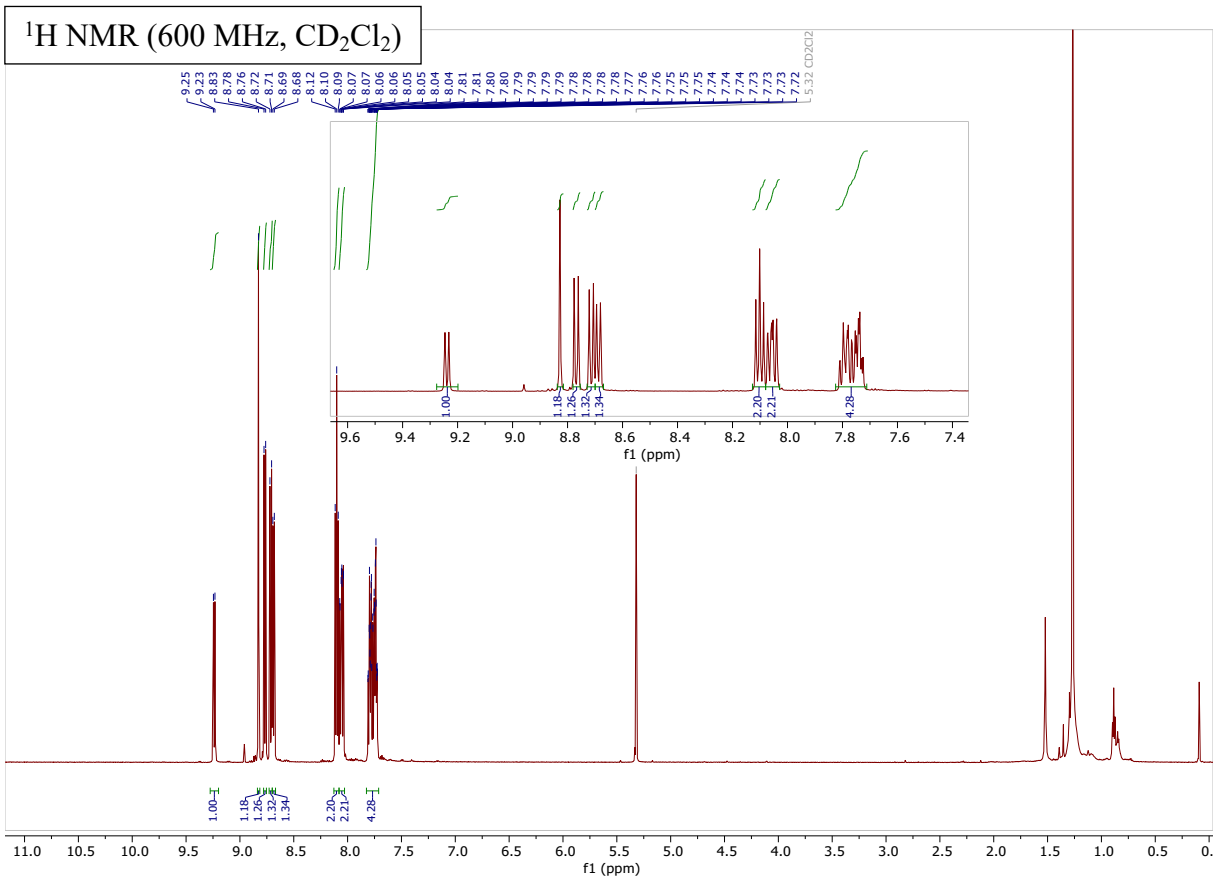

Figure S1. ^{1}H NMR of compound **S1**.

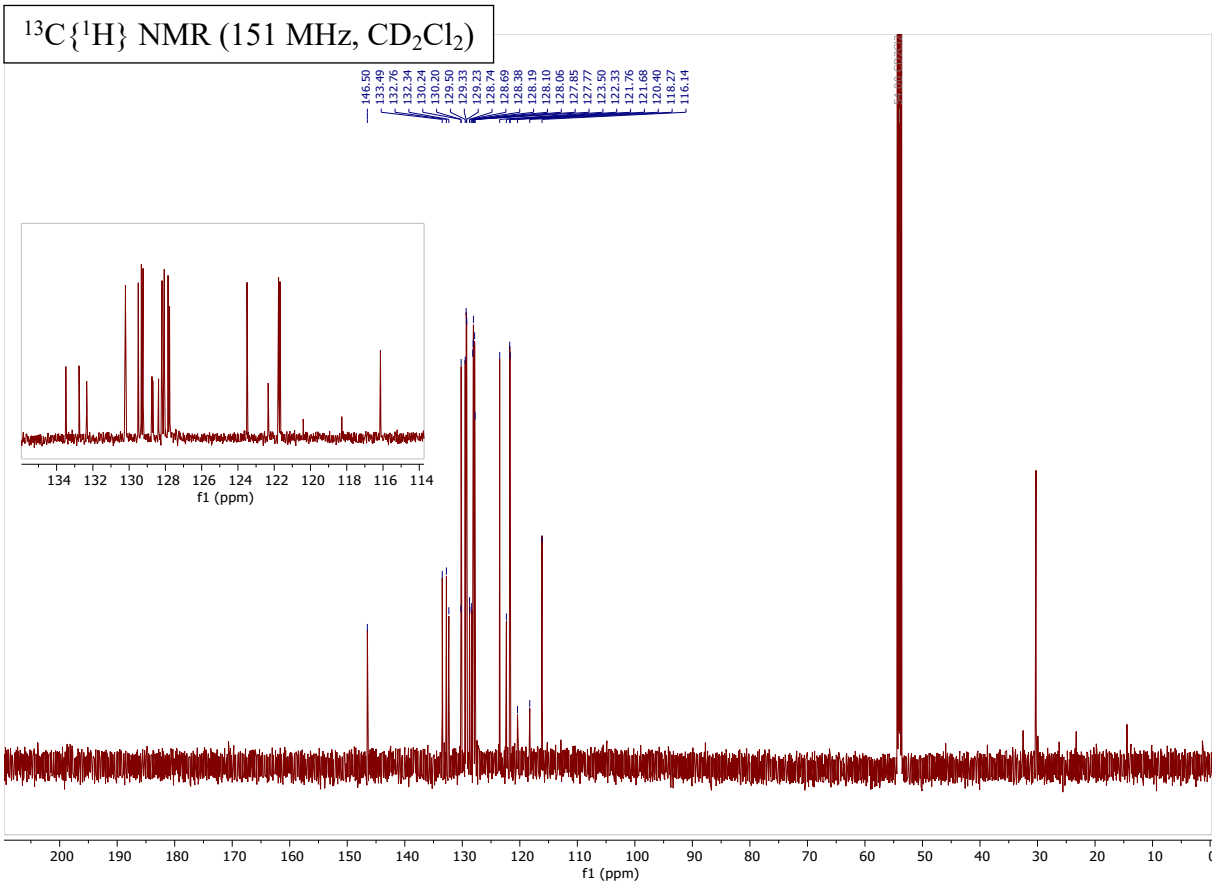

Figure S2. $^{13}C\{^{1}H\}$ NMR of compound **S1**.

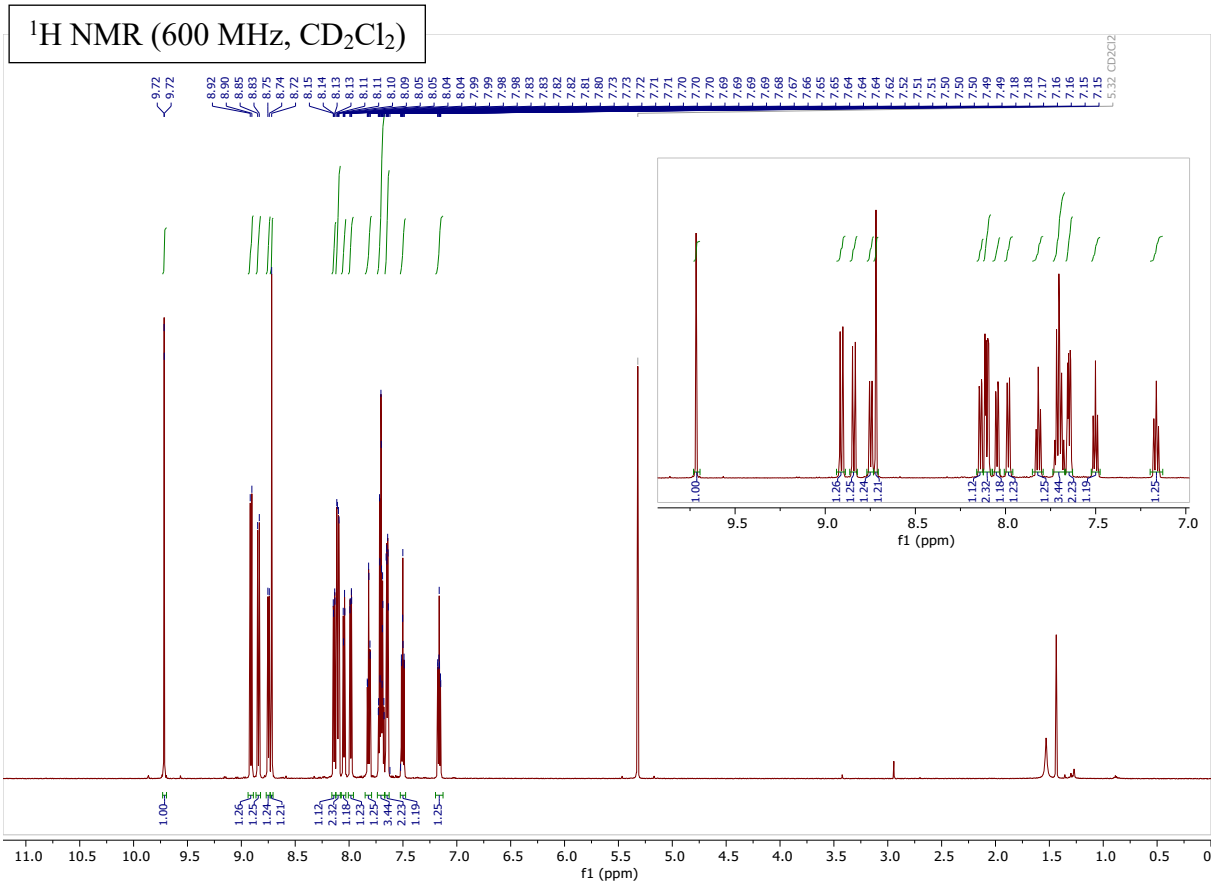

Figure S3. ^{1}H NMR of compound **1**.

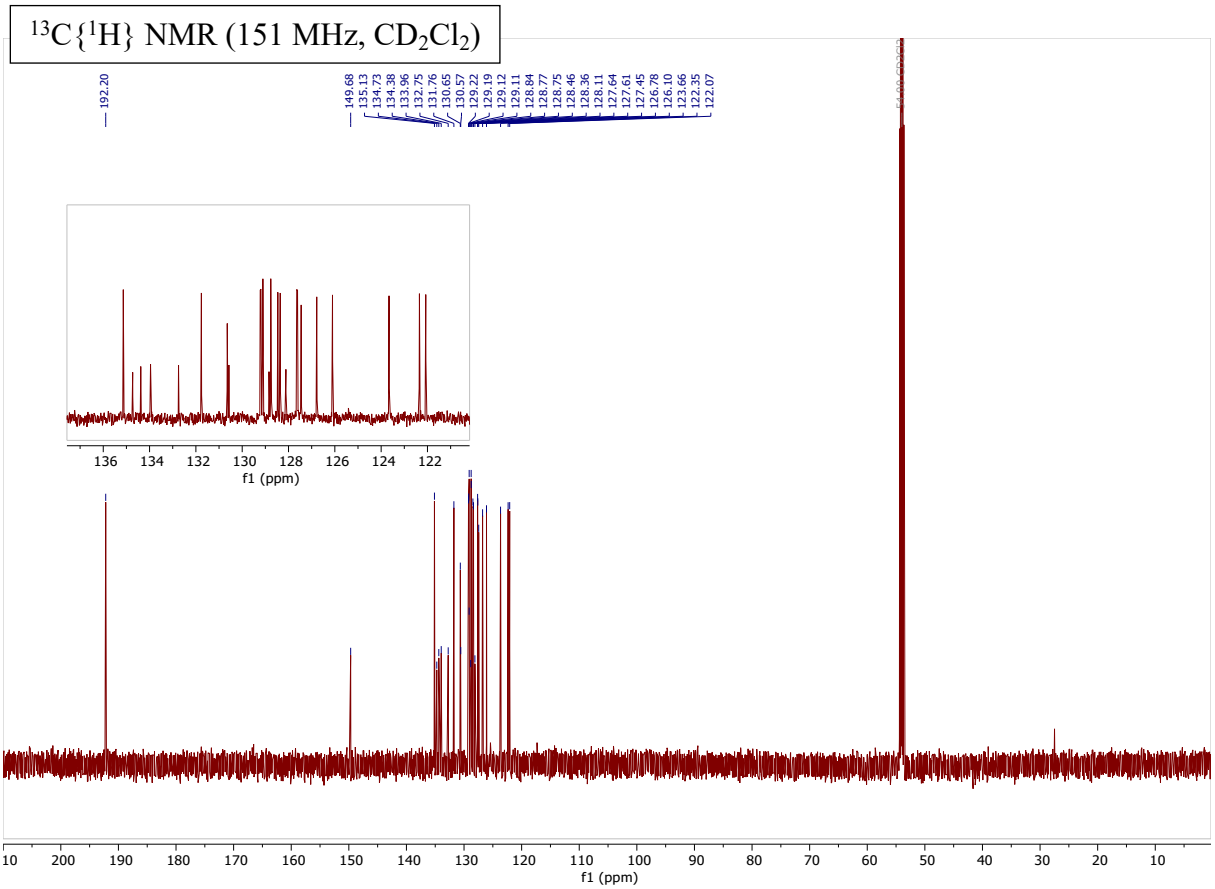

Figure S4. $^{13}C\{^{1}H\}$ NMR of compound **1**.

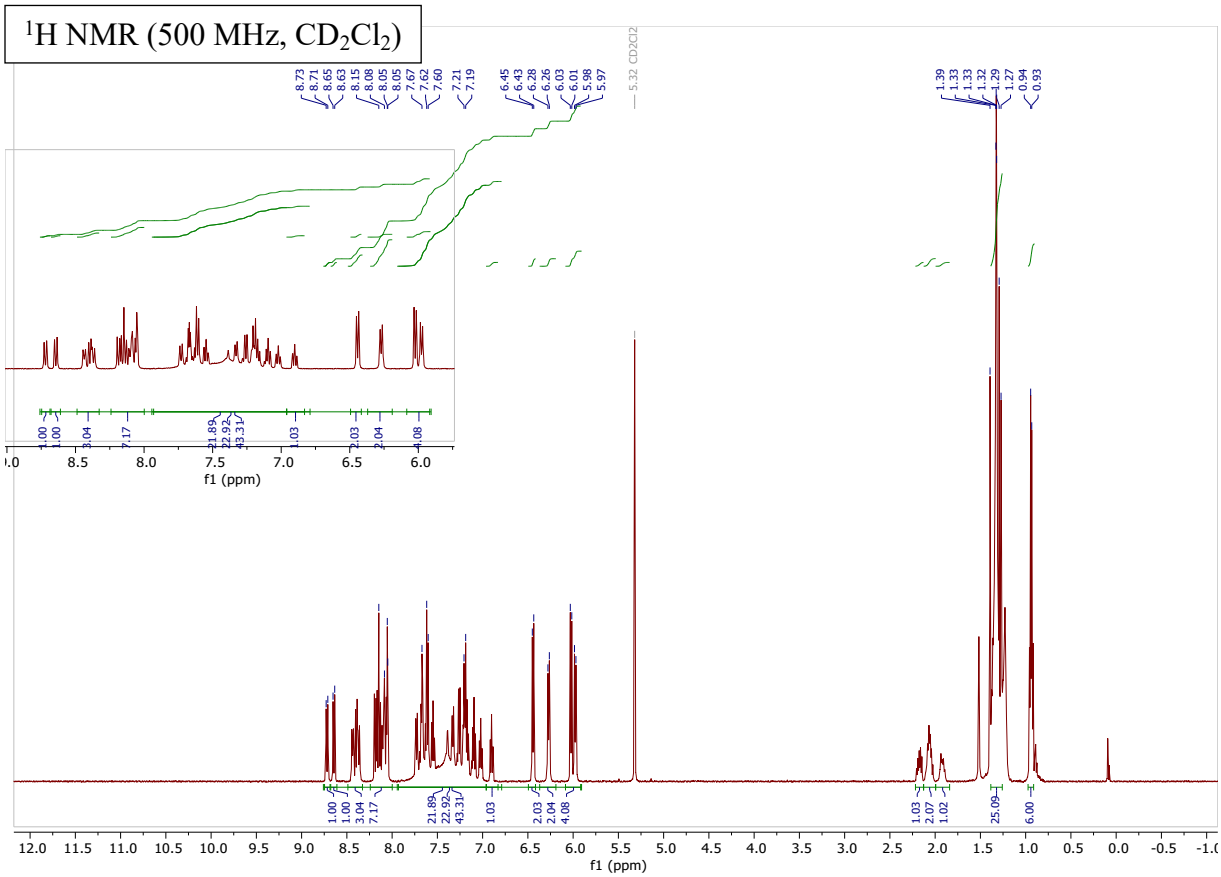

Figure S5. ^{1}H NMR of compound **2**.

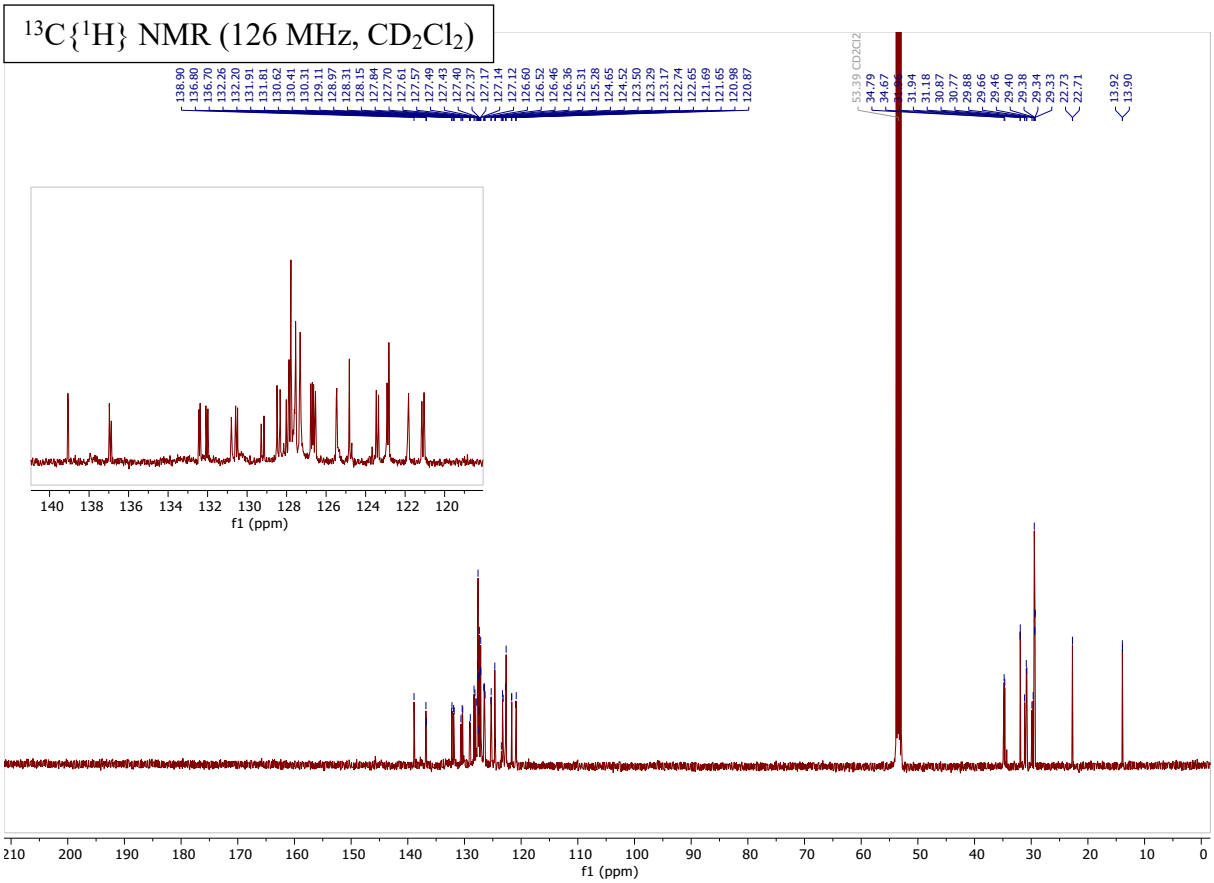

Figure S6. $^{13}C\{^{1}H\}$ NMR of compound **2**.

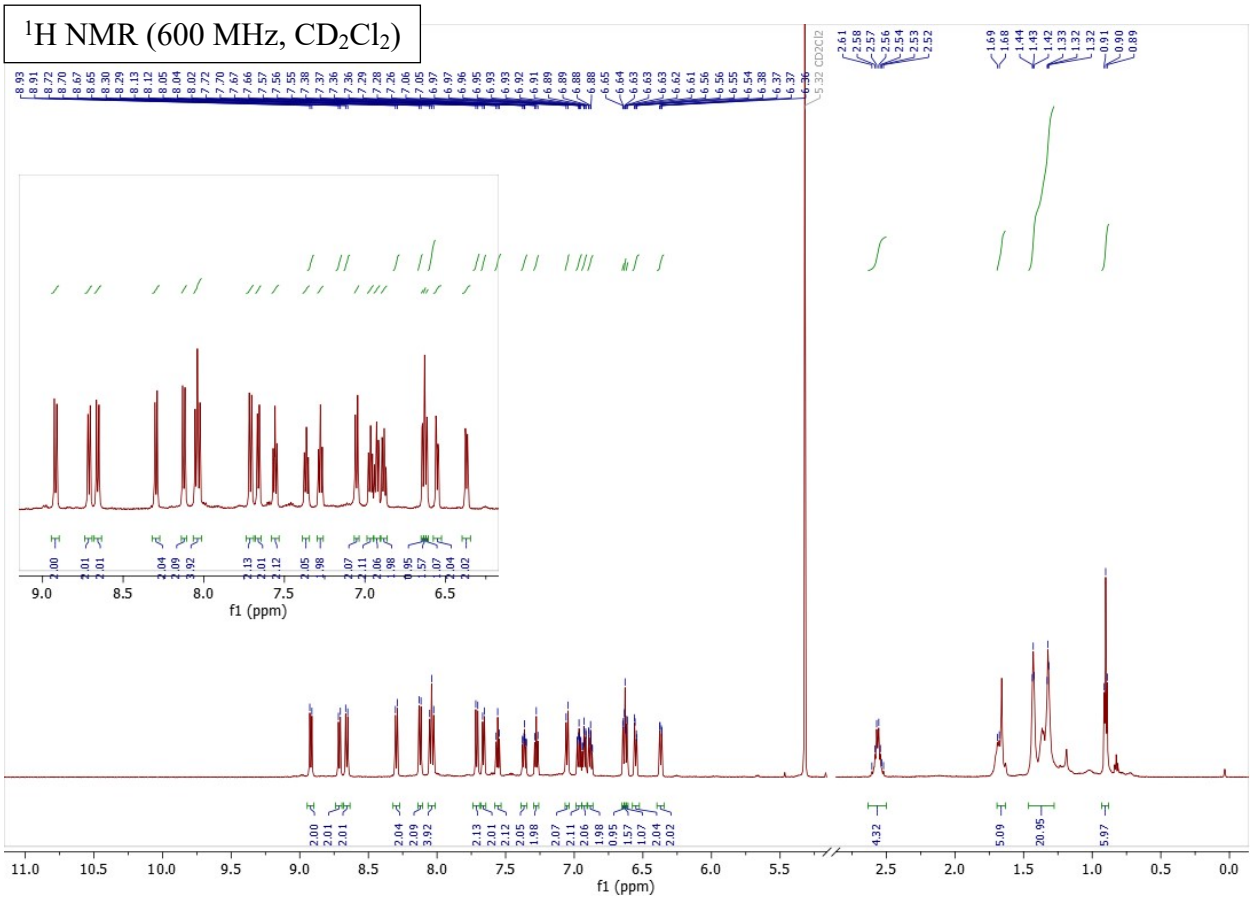

Figure S7. ^{1}H NMR of meso form of compound **4**.

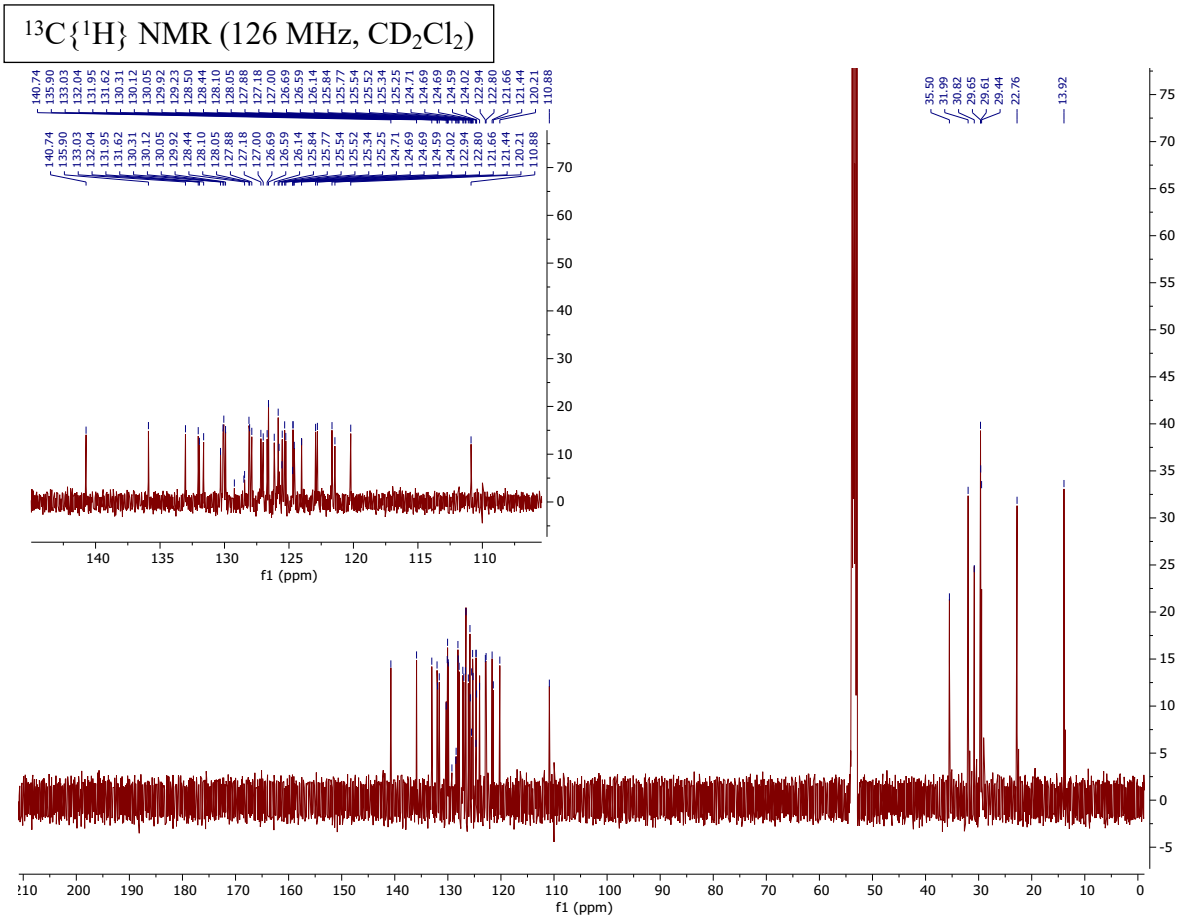

Figure S8. $^{13}C\{^{1}H\}$ NMR of meso form of compound **4**.

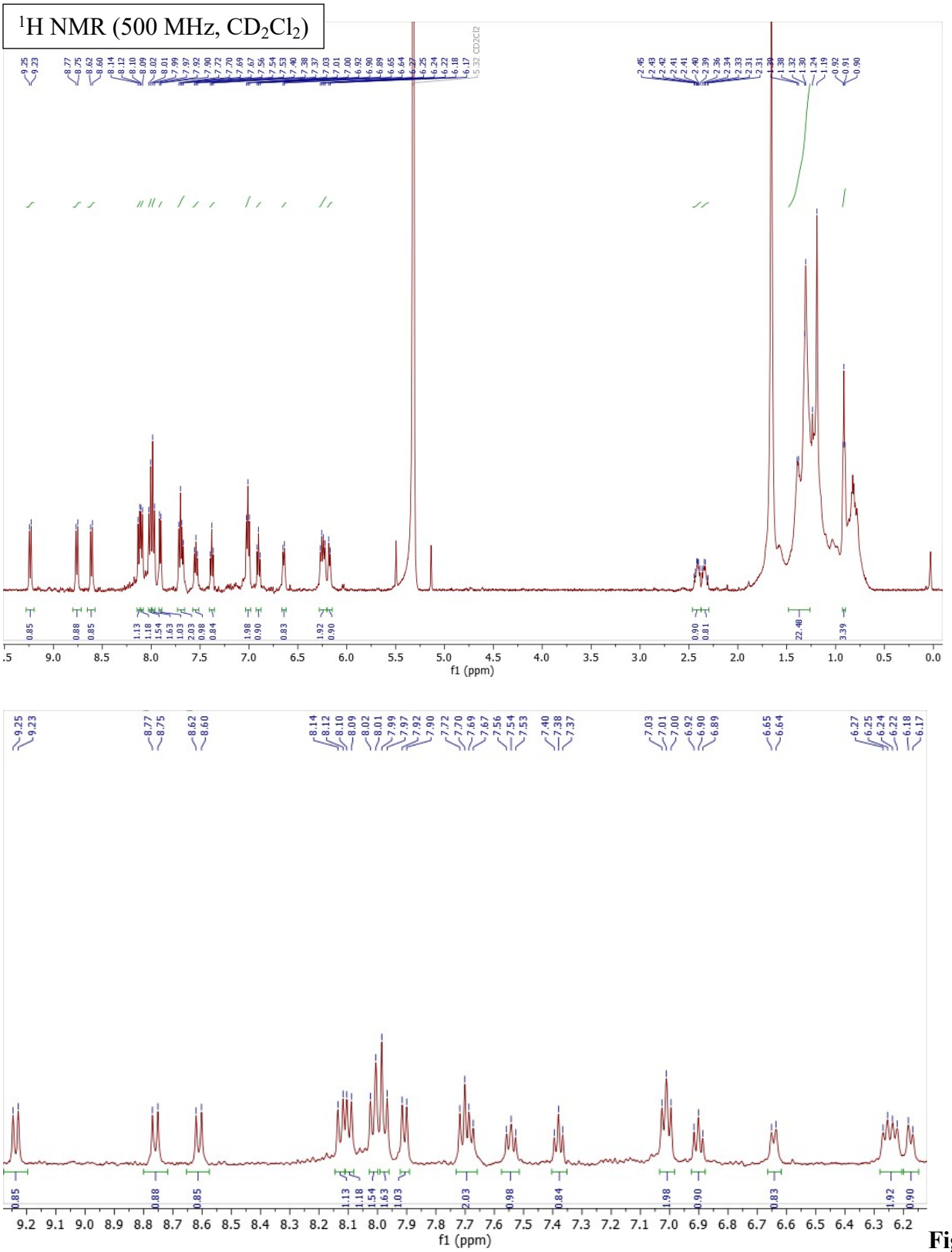

Figure S9. ^{1}H NMR of enantiomeric form of compound **4** and zoom of aromatic range.

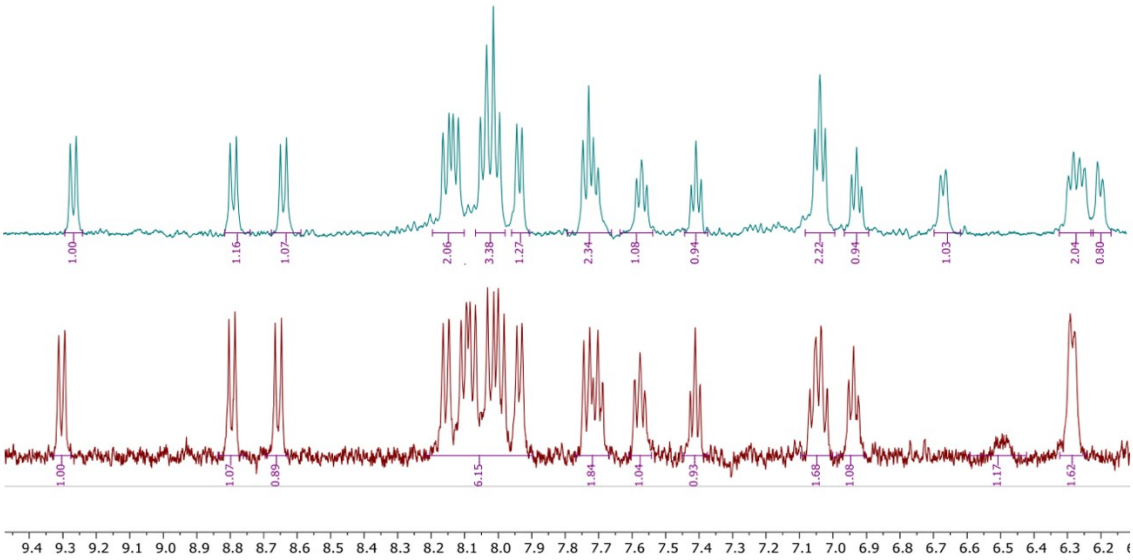

Figure S10. Comparison of aromatic signals for enantiomeric form of **4** in different temperatures (-40°C green colour, room temp. red colour).

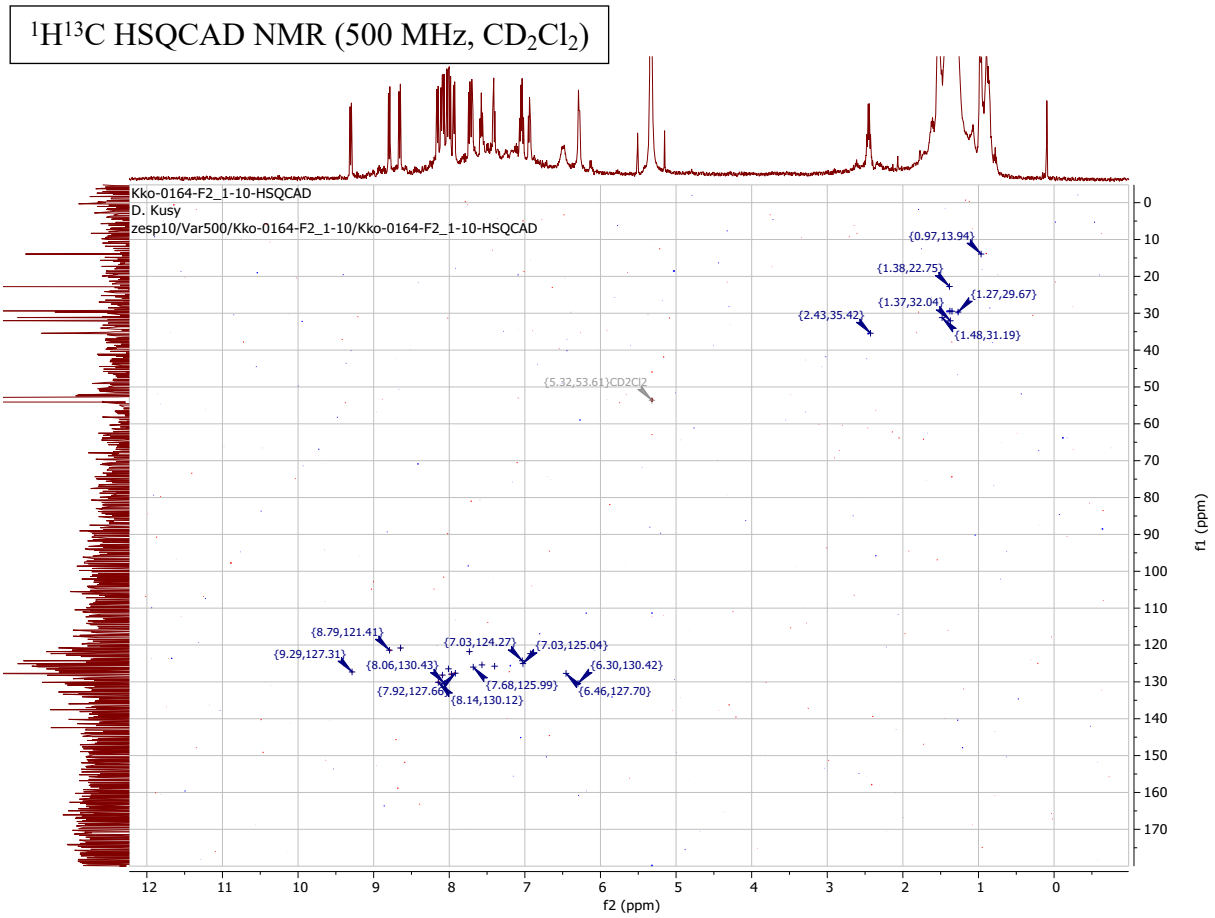

Figure S11. HSQCAD experiment of enantiomeric form of compound **4**. Due to low signal-to-noise ratio quaternary carbon atoms were not identified.

4. Chiral HPLC

Two samples of **4** are dissolved in dichloromethane, injected on the chiral column, and detected with a UV detector at 254 nm. The flow-rate is 1 ml/min.

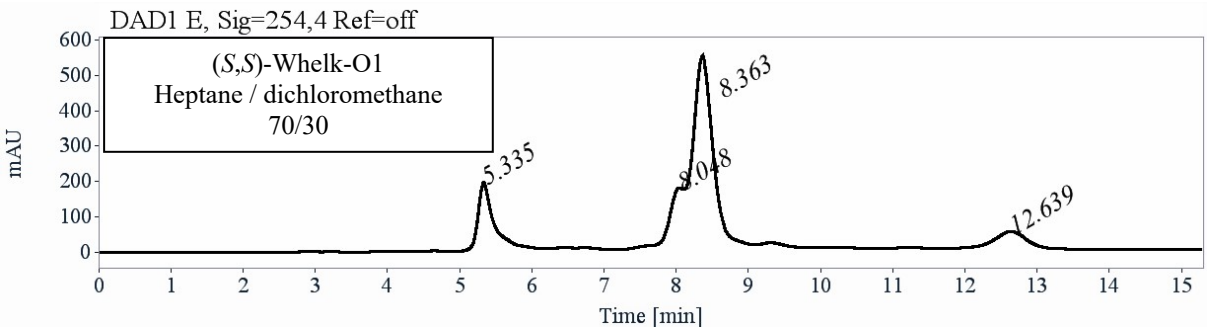

RT [min]	Area	Area%	Capacity Factor	
5.33	2930	16.93	0.81	First enantiomer
8.05	2249	13.00	1.73	Second enantiomer
8.36	10518	60.77	1.83	Meso ?
12.64	1610	9.30	3.28	Impurity
Sum	17307	100.00		

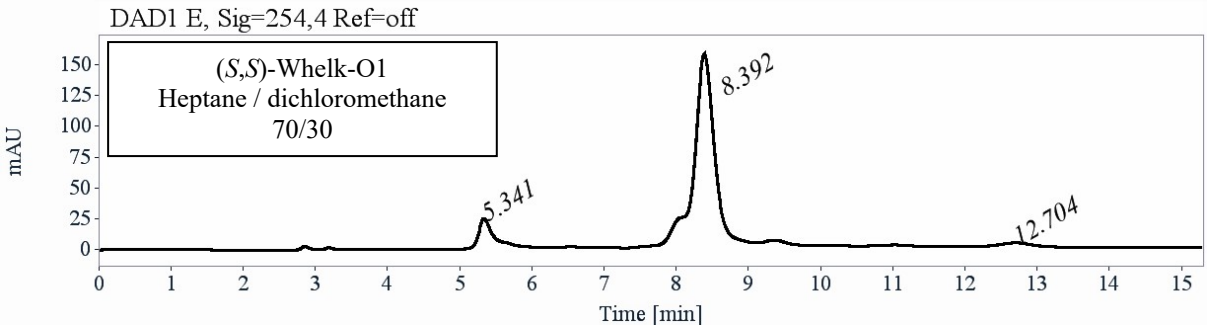

RT [min]	Area	Area%	Capacity Factor	
5.34	383	10.77	0.81	First enantiomer
8.39	3063	86.15	1.84	Second enantiomer and meso ?
12.70	109	3.07	3.31	Impurity
Sum	3555	100.00		

Preparative separation of first sample of **4**:

• Sample preparation: About 12 mg of compound **4** are dissolved in 7 mL of a mixture of dichloromethane and hexane (70/30).
• Chromatographic conditions: (*S*,*S*)-Whelk-O1 (250 x 10 mm) and (*R*,*R*)-Whelk-O1 (250 x 10 mm), hexane / dichloromethane (70/30) as mobile phase, flow-rate = 5 mL/min, UV detection at 254 nm.

• First enantiomer: 1.9 mg
• Second enantiomer: 1.3 mg
• Meso?: 2.6 mg
• impurity: 0.7 mg
• Intermediate 1: 3 mg
• Intermediate 2: 2 mg

Preparative separation of second sample of **4**:

• Sample preparation: About 12.5 mg of compound **4** are dissolved in 5 mL of a mixture of dichloromethane and hexane (70/30).
• Chromatographic conditions: (*S*,*S*)-Whelk-O1 (250 x 10 mm), hexane / dichloromethane (70/30) as mobile phase, flow-rate = 5 mL/min, UV detection at 254 nm.
• Injections (stacked): 25 times 200 µL, every 14 minutes.

• First enantiomer: 0.7 mg
• Second enantiomer + meso + impurities: 3.9 mg
• impurity: 0.7 mg
• Intermediate: 7 mg

Optical rotations

Optical rotations were measured on a Jasco P-2000 polarimeter with a halogen lamp (589, 578 and 546 nm), in a 10 cm cell, thermostated at 25°C with a Peltier controlled cell holder.

λ (nm)	Kko-0164-10 first eluted on (*S*,*S*)-Whelk-O1 $[\alpha]_\lambda^{25}$ (CH_2Cl_2, c = 0.063)	Kko-0164-10 second eluted on (*S*,*S*)-Whelk-O1 $[\alpha]_\lambda^{25}$ (CH_2Cl_2, c = 0.0675)
589	+ 260	- 260
578	+ 243	- 243
546	+ 87	- 87

5. Absorption and fluorescence

UV-Vis absorption spectra and emission spectra were recorded in toluene, dichloromethane and in 1 cm × 1 cm quartz cuvettes at room temperature, with spectrophotometer and spectrofluorometer, respectively. Dilute solutions ($c \approx 10^{-6}$ M) were used to avoid aggregation and inner-filter effects in emission spectra. Emission spectra were obtained upon excitation at 375 nm for **1-3**. To determine the fluorescence quantum yield in solution, a 9,10-diphenylantracene solution in toluene under air was used as a standard ($\Phi_{FL} = 0.70$).

6. X-ray crystallography

Single crystals suitable for X-ray measurements were grown using the diffusion method of MeOH into $CHCl_3$. Data collection was performed using a Bruker D8 Venture single crystal diffractometer equipped with a molybdenum anode X-ray tube ($\lambda = 0.71073$ Å), a CMOS detector, and a low-temperature attachment. Images containing reflections were recorded by means of APEX3[2], and data integration and reduction were carried out using SAINT.[3] The crystal structure was solved with SHELXT[4] implemented in Olex2[5] and refined with SHELXL.[6] The unit cell contains three molecules, A, B, and C, located at three inversion centres. Therefore, there are three halves of these molecules in the asymmetric unit. In all symmetrically independent halves of the molecules, there is disorder of the n-octyl substituents. This disorder was described by three (SOFs: 0.597, 0.218 and 0.185), three (SOFs: 0.582, 0.327 and 0.091) and two orientations (SOFs: 0.583 and 0.417) for A, B and C, respectively. The asymmetric unit also contains one chloroform molecule, a chloroform molecule with non-integer occupancy (SOF: 0.211), a hexane molecule with half-occupancy and disordered over three positions (SOFs: 0.318, 0.132 and 0.050), and an ethanol molecule with half-occupancy and disordered over four positions (SOFs: 0.234, 0.093, 0.092 and 0.081). The *n*-octyl substituent with the lowest occupancy in molecule B, the atoms of two orientations of the n-hexane molecule, and the atoms of three orientations of the ethanol molecule were refined isotropically. The remaining non-hydrogen atoms were refined in an anisotropic model. Hydrogen atoms were located geometrically and refined as riding with isotropic atomic displacement parameters set to be either 1.2 or 1.5 times larger than Ueq of the parent atom. Due to the strong disorder of n-octyl substituents and solvent molecules, restraints were imposed on bond lengths, valence angles, and atomic displacement parameters of these fragments and molecules. Selected experimental and crystal data are presented in Table S1. Full details can be found in the cif file.

Table S1. Data collection and structure refinement parameters.	
Formula	$C_{90}H_{74}N_2$ x 0.81$CHCl_3$ x 0.33C_6H_{14} x 0.33C_2H_5OH
M_x [g mol^{-1}]	1322.33
Crystal size [mm]	0.35 x 0.10 x 0.10
T [K]	130.0(5)
λ [Å]	0.71073
Crystal system	triclinic
Space group	$P\bar{1}$
a [Å]	15.5568(12)
b [Å]	20.3308(16)
c [Å]	20.5121(17)
α [°]	101.392(3)
β [°]	102.858(3)
γ [°]	104.546(3)
V [Å^3]	5897.3(8)
Z	3
Z'	1.5
D_x [Mg m^{-3}]	1.117
F(000)	2096
μ [mm^{-1}]	0.143
θ_{max} [°]	26.000
h_{max}, k_{max}, l_{max}	19, 25, 25
Reflections collected	194503
Reflections unique	23138
Reflections unique observed	16540
Completeness	0.999
R_{int}	0.0714
Refinement method	Full-matrix LSQ on F^2
R_1 for I>2σ(I)	0.0783
wR_2 for I>2σ(I)	0.2224
R_1 for all data	0.1076
wR_2 for all data	0.2494
GOF on F^2	1.039
$\Delta\rho_{max}$ [eÅ^{-3}]	0.747 (near hexane)
$\Delta\rho_{min}$ [eÅ^{-3}]	-0.612 (near octyl)

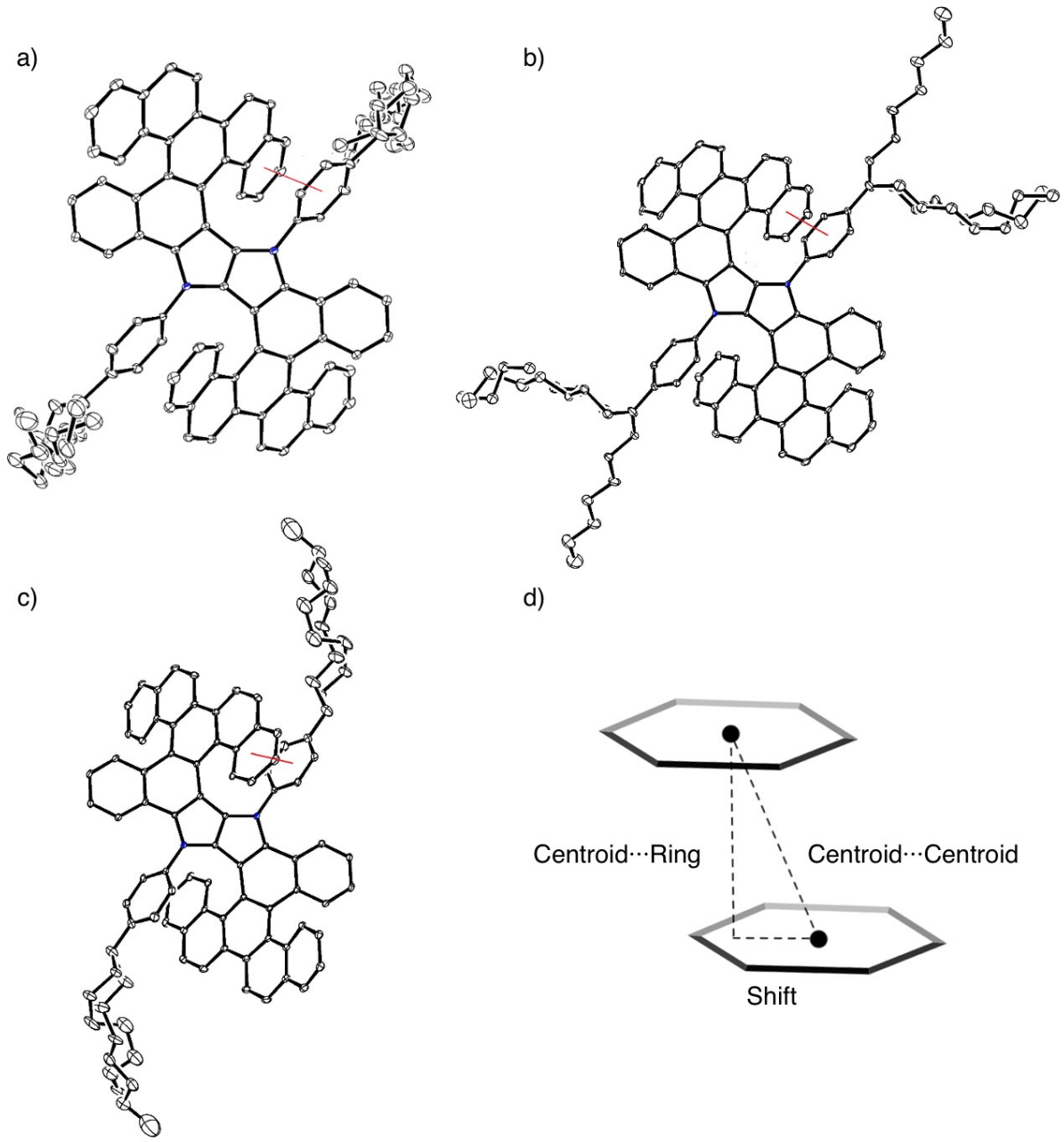

Figure S12. Molecules a) A, b) B, c) C and d) graphical representation of the parameters shown in Table S2. Only half of each molecule A, B and C is symetrically independent.

Table S2. Parameters for π-π stacking [Å].

Molecule	Centroid···Centroid	Centroid···Ring	Shift
A	3,476	3,208	1,338
B	3,527	3,175	1,536
C	3,633	3,082	1,924

Molecule A exhibits the strongest π-π stacking interactions, as indicated in Table S2.

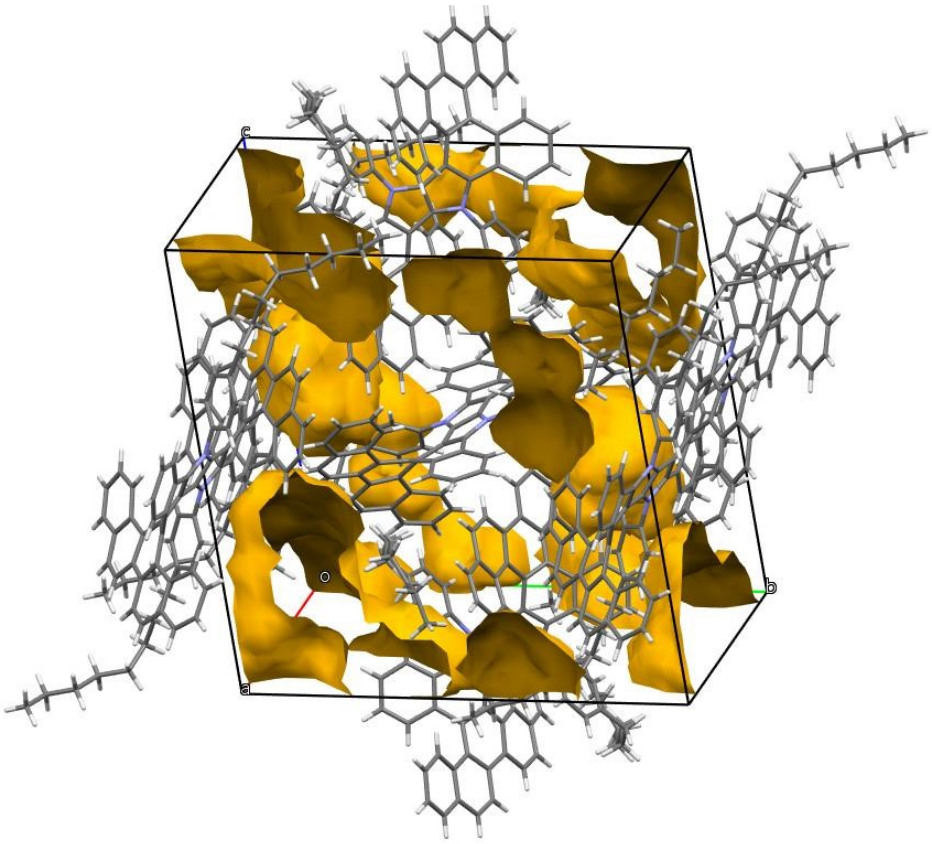

Figure S13. Packing of molecules in the unit cell of the meso form of compound **4**. Solvent molecules were omitted for clarity. The space occupied by solvent molecules is included in the yellow voids.

7. CD and CPL

CD spectra were measured on a JASCO J-1500 spectrometer equipped with a JASCO Peltier cell holder to maintain the temperature at 20.0 ± 0.2 °C. The pure solvent was used for baseline. The CD spectrometer was purged with nitrogen before recording each spectrum.

To acquire CPL spectra and obtain the corresponding dissymmetry factors (g_{lum}), a FLS1000 Edinburgh Instruments Fluorimeter, equipped with a PEM, a lock-in amplifier and an emission polarizer at 135°, was employed. The solutions were diluted as to have absorbance lower than 0.1, in order to minimize inner-filter effects. The absence of linearly polarized components in emission was confirmed by verifying that the CPL spectra did not change when excited through a horizontal polarizer. CPL spectra were recorded by exciting the sample at 405 nm, despite its low absorbance at this wavelength, because the excitation source in our fluorometer (a Xenon lamp) has very low emission power in the UV, while much higher output in the visible region. The excitation wavelength of 405 nm was a good tradeoff between source emission and sample absorption, thus allowing to maximize the intensity of the collected signal. The B_{CPL} was calculated using the molar extinction value at 320 nm, i.e. at the absorption peak closer to the visible region.

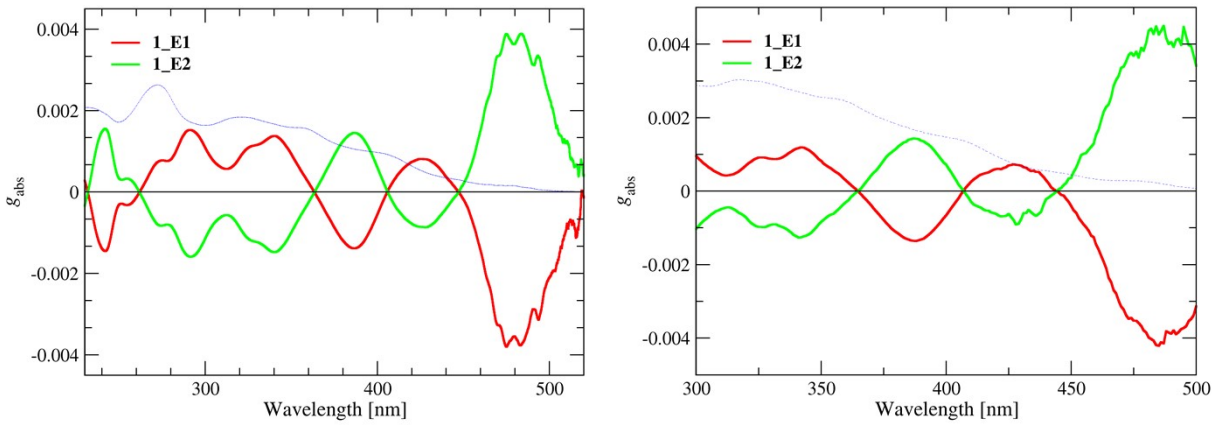

Figure S14. Full red and green lines: absorption dissymmetry factor (g_{abs}) of the two enantiomers of compound **4** in DCM (left panel) and in toluene (right panel). The absorption spectrum is reported as a blue thin line, as a reference to locate the transitions.

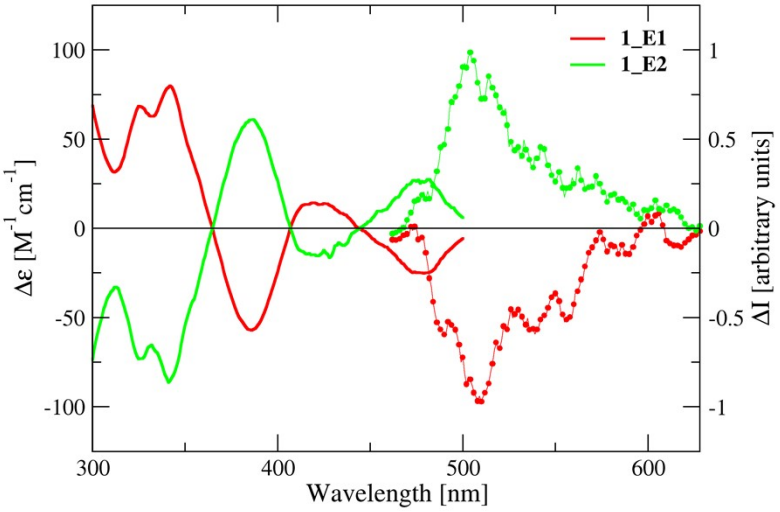

Figure S15. CD (solid lines) and CPL (dotted lines) spectra of the enantiomers of **4** in toluene.

8. Computational methods

Peak Fitting of the Experimental Spectra.

The experimental ECD and UV spectra recorded in dichloromethane have been fitted by sums of Gaussians. The resulting model spectra (magenta) are hardly distinguishable from the experimental curves (Figures S16-S17). Due to the presence of broad overlapped bands, the number and the location of the peaks in the two spectra can differ. Nevertheless, a very good agreement is achieved for 4 out of the 8 model peaks of the UV spectrum, which are found almost unchanged in the model of the ECD spectrum.

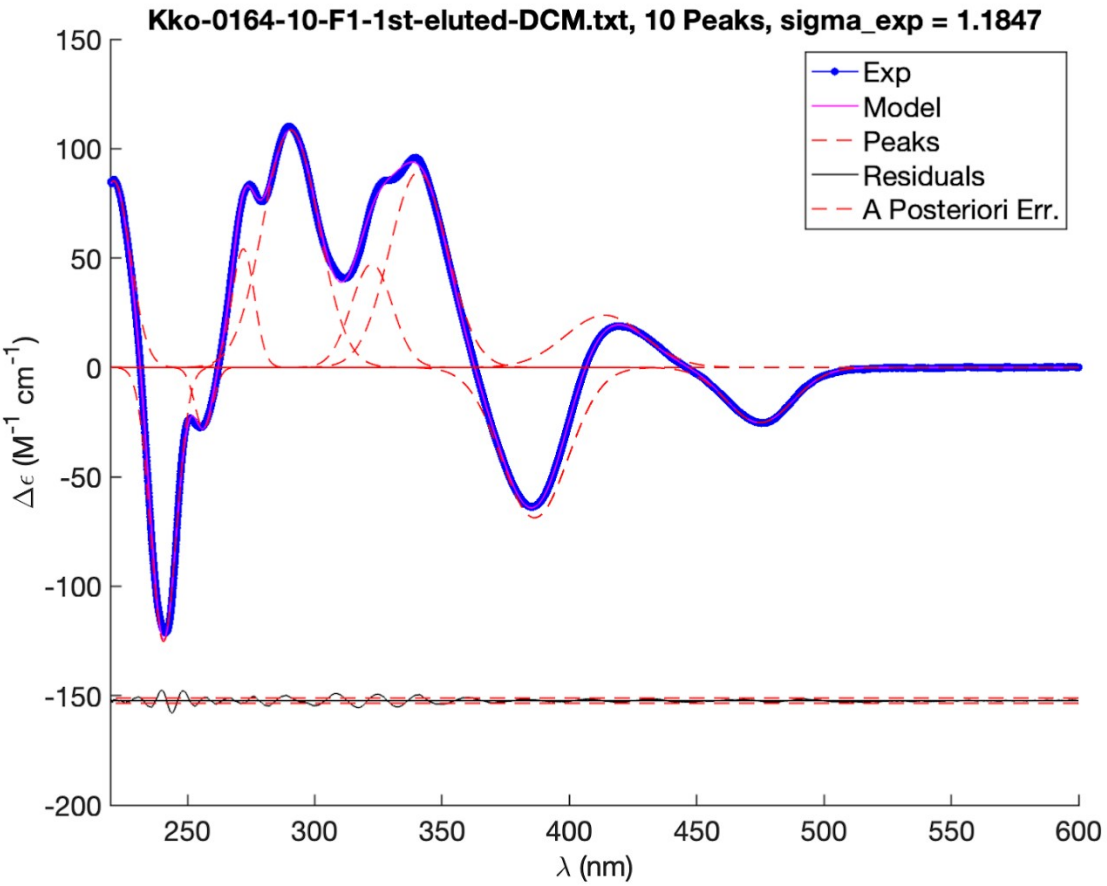

Figure S16. ECD in DCM of the first eluted fraction of diazahelicene. Comparison of experimental curves with a fitting model (magenta) obtained as a summation of Gaussian functions. The homoskedastic a posteriori error is given as a dashed line on top of the arbitrarily down-shifted residuals.[7]

The full-width-at-half-maximum (FWHM) of the Gaussians used ranges between 0.15 and 0.39 eV, with a mean of 0.23 eV and a median of 0.22 eV.

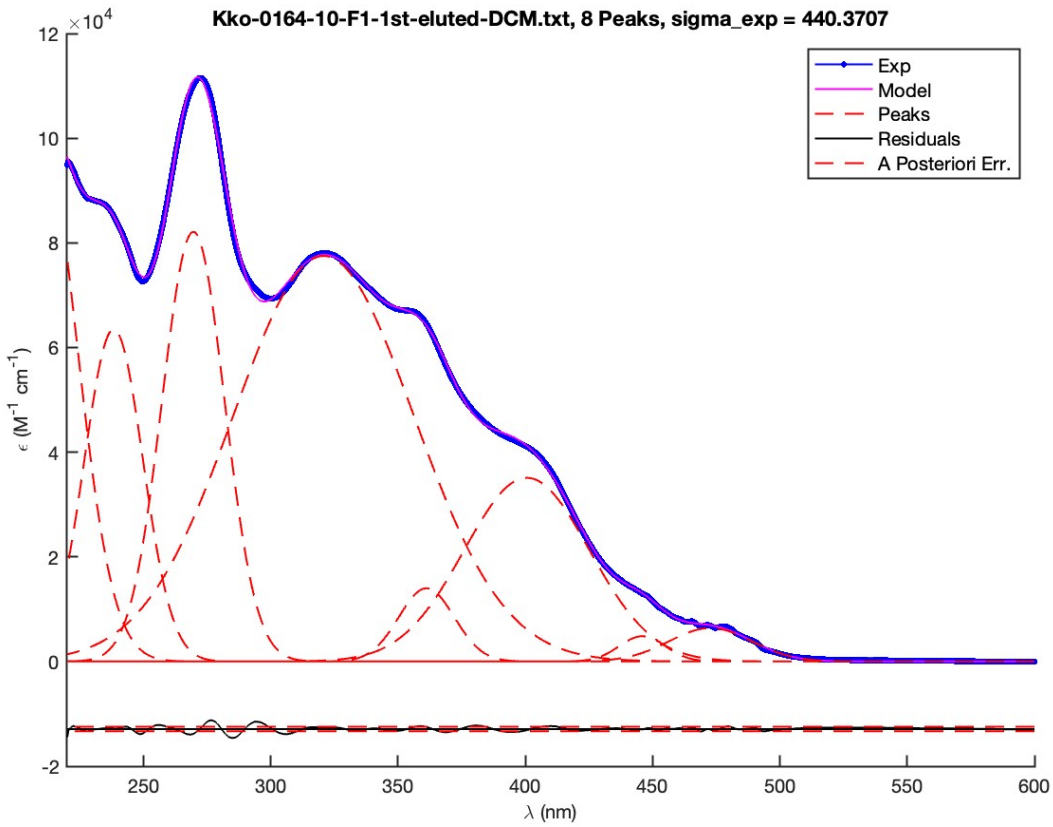

Figure S17. UV spectrum in DCM of the first eluted fraction of diazahelicene. Comparison of experimental curves with a fitting model (magenta) obtained as a summation of Gaussian functions. The homoskedastic a posteriori error is given as a dashed line on top of the arbitrarily down-shifted residuals.[7]

Table S3. Spectral parameters obtained by non-linear fitting of the UV (8 peaks, first 3 columns) and ECD (10 peaks, last 2 columns) spectrum. The peaks marked with a star have good correspondence of location between UV and ECD.

λ (nm)	*D* (au)	*f*	λ (nm)	*R* (au)
*472.7	0.7823	0.0503	474.8	-0.0841
446.0	0.3507	0.0239	413.8	0.1082
400.6	7.6848	0.5827	386.4	-0.2839
361.2	1.5047	0.1265	340.7	0.3631
*320.7	30.5382	2.8921	322.4	0.1436
			290.6	0.4986
*269.6	13.3634	1.5058	271.9	0.1058
			256.4	-0.0466
*238.3	10.9346	1.3939	240.6	-0.3199
209.4	24.6271	3.5716	221.1	0.3081

DFT computations have been performed using Gaussian 16.[8] Geometry optimization has been performed using the BP86 functional, which is generally a reliable choice for geometry optimizations, and it has been successfully applied to corrole systems.[9] On the other hand, a recent investigation has shown that the ωB97X-D functional[10] best performs for the calculation of vertical excitation energies among a set of more than 40 functionals.[11] Since solvent corrections should also be included, we here adopted the two protocols ωB97X-D/TZVP-PCM//ωB97X-D/TZVP-PCM and ωB97X-D/TZVP-PCM//BP86-D3/TZVP-PCM. In both cases, the TD-DFT algorithm was requested to compute the first 200 excited states.

Energies

Table S4. Sketches of conformers and their relative internal (*E*) and free (*G*) energy, in kcal mol^{-1}, computed at the BP86-D3/TZVP-PCM and ωB97X-D/TZVP-PCM//BP86-D3/TZVP-PCM levels, for the PP configuration of the central *aza*helicenes.

		BP86		wB97xD//BP86
Conf.		*E*	*G*	*E*
M,PP,M	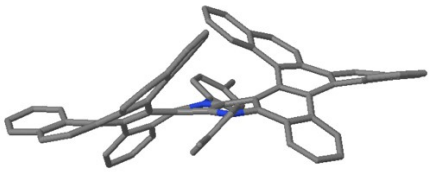	0.000	0.368	0.654
M,PP,P	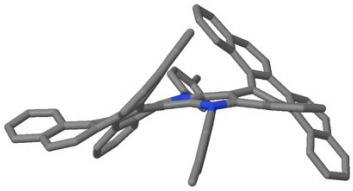	1.540	1.312	1.693
P,PP,M	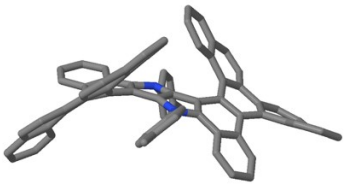	1.540	1.312	1.693
P,PP,P	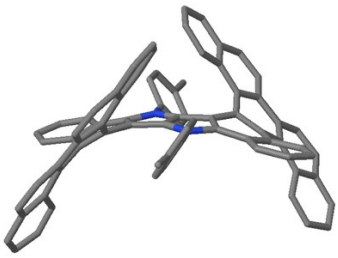	1.007	0.000	0.000

Table S5. Sketches of conformers and their relative internal (*E*) and free (*G*) energy, in kcal mol^{-1}, computed at the BP86-D3/TZVP-PCM and ωB97X-D/TZVP-PCM//BP86-D3/TZVP-PCM levels, for the PM configuration of the central *aza*helicenes. At the BP86-D3/TZVP-PCM level, the energy of the P,PM,M conformation is 1.471 kcal mol^{-1} below the energy of the M,PP,M conformation reported in Table S4, and its free energy is 1.539 kcal mol^{-1} below the free energy of conformation P,PP,P reported in Table S4. At the ωB97X-D/TZVP-PCM//BP86-D3/TZVP-PCM level, the energy of the P,PM,M conformation is 2.274 kcal mol^{-1} below the energy of the P,PP,P conformation reported in Table S4.

		BP86		wB97xD//BP86
Conf.		*E*	*G*	*E*
P,PM,M	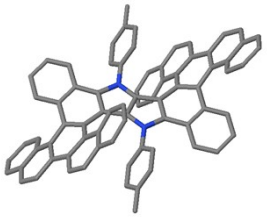	0.000	0.000	0.000

P,MP,P	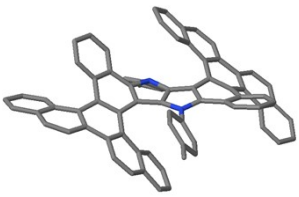	8.855	9.176	10.214
P,MP,M	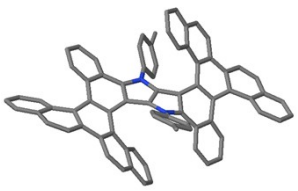	13.528	13.762	15.641

Table S6. Calculated and experimental chemical shifts (ppm) relative to TMS of aromatic protons of the P,PP,P atropisomer of **4**. The experimental multiplicity, the number and a color code are also given: the grey color is for the H atoms whose signal undergo significant changes upon a change of temperature. Calculations have been performed at the B972/6-311+G(2d,p)-PCM level using the CSGT approach for the calculation of the magnetic properties. The TMS

isotropic shielding has been set as 31.3885 ppm, which is the sum of the isotropic shielding (24.0285 ppm) and experimental chemical shift (7.36 ppm) for the protons of benzene (in DCB).

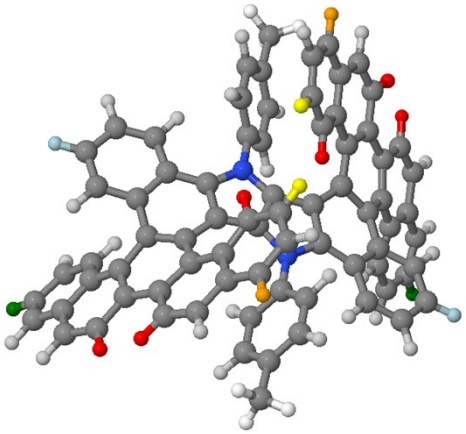

Calc.	Exp.	Mult.	#	color
9.70	9.24	d	2	
9.25	8.76	d	2	
9.10	8.61	d	2	
8.41	8.13-7.96	m	10	
8.37				
8.34				
8.22				
8.22				
8.19	7.91	d	2	
8.18	7.74 – 7.65	m	4	
7.81				
7.74	7.54	t	2	
7.62	7.38	t	2	
7.23	7.01	t	4	
7.18				
7.13	6.9	t	2	
6.97	6.64	d	2	
6.93	6.26	d	2	
6.40	6.23	d	2	
6.26	6.18	d	2	

ECD Spectra

The ECD spectra of the 3 conformers, each computed as sum of Gaussians with FWHM of 0.25 eV, show that the main source of chirality is the central portion of the molecule: the different chiralities of the lateral [5]helicene moieties basically cause small shifts in intensity and position of the dichroic bands, and only change the sign of the spectrum in the middle part of the spectrum.

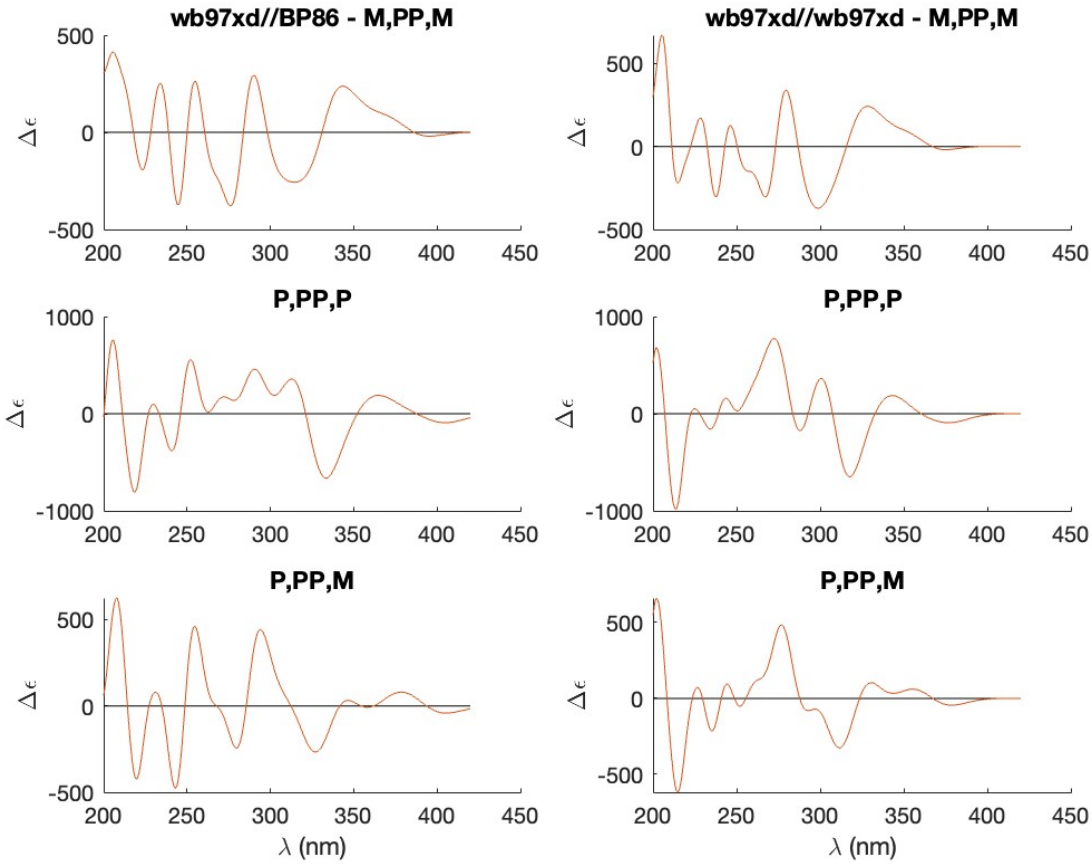

Figure S18. TD-DFT ECD spectra for the 3 conformers computed at the ωB97X-D/TZVP-PCM//BP86-D3/TZVP-PCM level (left) and at the ωB97X-D/TZVP-PCM//ωB97X-D/TZVP-PCM (right), assuming Gaussian functions with HWFM of 0.25 eV.

Compared to the experimental ECD spectrum, all computed spectra exhibit a degree of blue-shift, particularly pronounced in the ωB97X-D//ωB97X-D calculation. According to this, we will focus in the following on the ωB97X-D//BP86-D3 calculations, which combines the spectral data computed with the ωB97X-D functional with the free energies computed with the BP86-D3 functional. While many DFT methods are known to systematically produce red-shifted excitation energies, blue-shifted predictions are also reported.[12] The ωB97X-D in particular has been reported to yield to very small systematic error.[11] However, benchmarks on small molecules do not necessarily predict the outcomes on any single molecule, especially on a large system like the one considered here, and one should consider that root-mean-squared error on the energy transitions typically amounts to several tenths of an electronvolt. Moreover, a recent investigation on a double helicene built on the same 1,4-dihydropyrrolo[3,2-*b*]pyrrole core reported a similar blue shift of the spectrum computed with a different functional as compared to the experimental one.[13] For that reason, to allow for a meaningful comparison between computed and experimental spectra, we introduced a systematic energy shift of all transitions. In more detail, we proceeded as follows:

1) **Systematic energy shift:** we shifted all transitions of all conformers by a constant amount in the range $\Delta E \in$ [-0.5 eV, +0.5 eV], a range which is roughly equal to the 95% probability interval assuming a Gaussian distribution of the errors out of the RMSE values published by Liang *et al*.[11]

2) **Spectral generation:** for each value of the energy shift ΔE, we obtained DFT spectra by convoluting the transitions with Gaussian functions with a FWHM of 0.25 eV. We either considered individual conformers, or their Boltzmann average at 298 K, using the computed free energy for thermal average, and taking into account the multiplicity of the 3 non-degenerate conformers (the P,PP,M conformer counts for 2 as it coincides with the M,PP,P one),

3) **Model comparison:** For each so-computed spectrum we compute the cosine similarity (COSI) and a scale factor SF as

$$COSI = \frac{y \cdot y^{DFT}}{\|y\| \|y^{DFT}\|},$$

$$SF = \frac{y \cdot y^{DFT}}{y^{DFT} \cdot y^{DFT}},$$

here vectors y and y^{DFT} contain the experimental and DFT values of the ECD spectrum, respectively. COSI is a robust goodness-of-fit indicator (GOFI), thus particularly effective for distinguishing models which are only in partial agreement with the data. A perfect model should have COSI = 1, while a model which just differs in sign from the data should have COSI = -1.

4) **Model selection:** we selected the value with maximum value of a positive COSI and for it we determined a model spectrum as $y^M = SF\, y^{DFT}$,

5) **Uncertainty estimation:** for the best model of each stable configuration, we obtained the standard deviations of the COSI via the bootstrap method, to safely identify the model that best fit the experimental values.[14]

The results of this procedure are summarized in Table S7, and the best matching spectra are shown in Figure S19 of the main paper. Both visual inspection and the values of the COSI, together with its error, leave no doubts on the better ability of model *,PP,* to reproduce the spectrum of the first eluted fraction of diazahelicene, allowing for its absolute configuration assignment.
Interestingly, the single conformer P,PP,P provides an even closer match to the experimental spectrum. This is likely due to limitations in the Boltzmann weighting procedure, which relies on free energies computed within the harmonic approximation.

Table S7. Results of the maximization of the COSI between model spectra and the experimental ECD spectrum of first eluted fraction of diazahelicene. Values in parentheses are the standard deviation of the COSI estimated by the bootstrap method.[14] In addition to the optimal COSI and its standard deviation, the table reports the energy shift ΔE and the scale factor SF.

Model	Δ*E* (eV)	SF	COSI
,MM,	0.50	0.079	0.21(2)
,PP,	-0.48	0.200	0.69(1)
M,MM,M	0.5	0.054	0.22(2)
P,MM,P	-0.2	0.129	0.38(2)
M,MM,P	0.47	0.070	0.19(2)
P,PP,P	-0.46	0.149	0.755(8)
M,PP,M	0.15	0.058	0.15(2)
P,PP,M	-0.47	0.163	0.56(2)

Table S8. Electronic and geometric properties of the most prominent electronic transitions, extracted from Gaussian 16 output. For each excited state, we report: the excitation energy (in eV and nm), the main contributing orbital excitations with their corresponding amplitudes (when there is at least an amplitude larger than 0.25), oscillator strength (*f*), rotatory strength (*R*, in velocity formalism, in 10^{-40} erg esu cm/gauss), the relative angle (in degrees) between electric and magnetic transition dipole moments.

State#	Symmetry	Vertical Energy, (eV / nm)	MOs contribution [Amplitude]	*f*	*R* (cgs)	Angle E-M (degrees)
1	B	3.104 / 399.5	H -> L [0.53] H-1 -> L+2 [0.23]	0.1468	-279	159
2	A	3.189 / 380.2	H -> L+1 [0.48] H-1 -> L+3 [0.20]	0.0393	161	0.01
5	B	3.473 / 357.0	H -> L+2 [0.47] H-2 -> L+3 [-0.31]	1.3880	66	87.42
7	B	3.754 / 330.3	H-1 -> L+2 [0.47] H -> L [-0.26]	1.1770	-1099	160.21
10	A	3.959 / 313.2	H-1 -> L+3 [0.41] H-2 -> L+2 [0.15]	0.4662	1111	0.03
16	A	4.332 / 286.2	H-2->L+4 [0.29]	0.5667	2414	0.02
17	B	4.363/ 284.16	-	0.3027	-2278	174.28
30	A	4.938 / 251.1	-	0.6078	1218	0.0

Figure S19. Frontier orbitals of P,PP,P azahelicene displayed with an isovalue=0.03 au.

HOMO (a) -6.80 eV	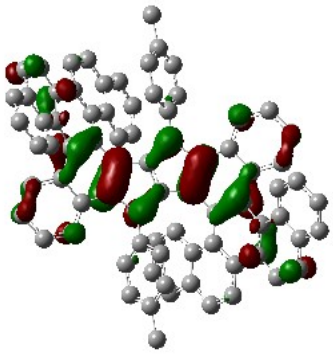	LUMO (b) -0.50 eV	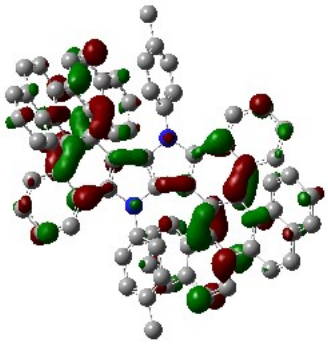
HOMO-1 (a) -6.94 eV	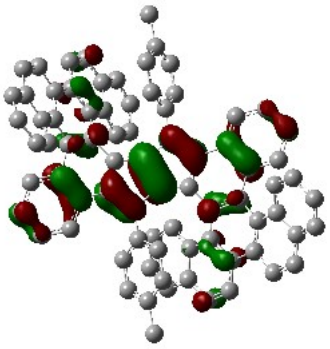	LUMO+1 (a) -0.35 eV	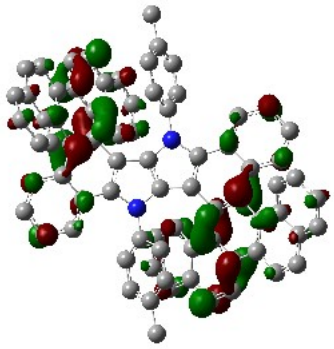
HOMO-2 (b) -7.29 eV	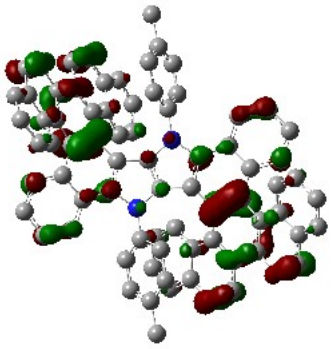	LUMO+2 (b) -0.24 eV	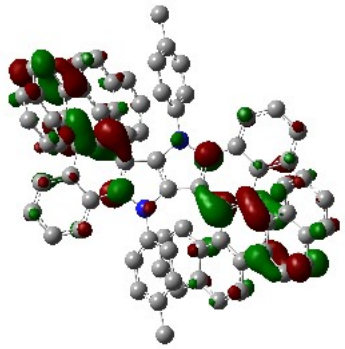

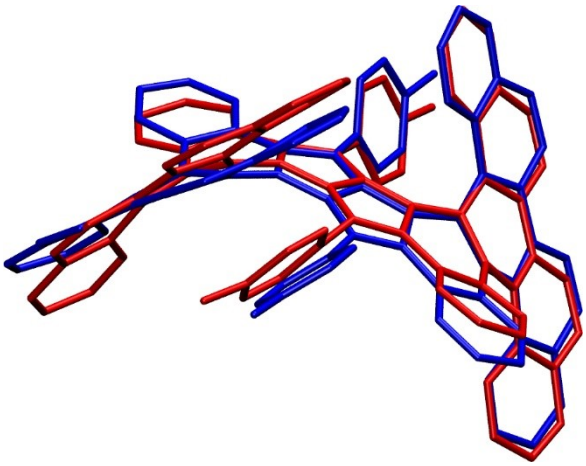

Figure S20. Superimposition of optimized structures for S_0 (blue) and S_1 (red). The RMSD between the two structures is 0.729 Å.

As for the dissymmetry factors, we computed g_{ABS} (H->L) in dichloromethane and in toluene, obtaining respectively $-8.992 \cdot 10^{-3}$ and $-8.993 \cdot 10^{-3}$, while for g_{LUM} (H->L) we obtained $-4.832 \cdot 10^{-3}$ in dichloromethane and $-4.762 \cdot 10^{-3}$ in toluene. The lower values for g_{LUM} as compared to g_{ABS} can be ascribed to an increase in the transition dipole moment at the excited state geometry.

9. References

(1) Lin, S.; You, T. An efficient one-pot approach to phenanthrene derivatives using a catalyzed tandem Ullmann-pinacol coupling reaction. *Tetrahedron*. 2008, *64* (42), 9906–9910 DOI:10.1016/j.tet.2008.08.004.
(2) APEX3 V2019, Bruker Nano, Inc., Software Package for the Solution of Crystal Structures, Madison, WI, USA. 2019. 2019.
(3) SAINT V8.40A, Bruker Nano, Inc., Software Package for the Solution of Crystal Structures, Madison, WI, USA,. 2019.
(4) Sheldrick, G. M. *SHELXT* – Integrated space-group and crystal-structure determination. *Acta Crystallogr. Sect. Found. Adv.* 2015, *71* (1), 3–8 DOI:10.1107/S2053273314026370.
(5) Dolomanov, O. V.; Bourhis, L. J.; Gildea, R. J.; Howard, J. A. K.; Puschmann, H. *OLEX2* : a complete structure solution, refinement and analysis program. *J. Appl. Crystallogr.* 2009, *42* (2), 339–341 DOI:10.1107/S0021889808042726.
(6) Sheldrick, G. M. Crystal structure refinement with *SHELXL*. *Acta Crystallogr. Sect. C Struct. Chem.* 2015, *71* (1), 3–8 DOI:10.1107/S2053229614024218.
(7) Monaco, G.; Aquino, F.; Zanasi, R.; Herrebout, W.; Bultinck, P.; Massa, A. Model-averaging of ab initio spectra for the absolute configuration assignment via vibrational circular dichroism. *Phys Chem Chem Phys*. 2017, *19* (41), 28028–28036 DOI:10.1039/C7CP05358D.
(8) Frisch, M. J.; Trucks, G. W.; Schlegel, H. B.; Scuseria, G. E.; Robb, M. A.; Cheeseman, J. R.; Scalmani, G.; Barone, V.; Petersson, G. A.; Nakatsuji, H.; Li, X.; Caricato, M.; Marenich, A. V.; Bloino, J.; Janesko, B. G.; Gomperts, R.; Mennucci, B.; Hratchian, H. P.; Ortiz, J. V.; Izmaylov, A. F.; Sonnenberg, J. L.; Williams-Young, D.; Ding, F.; Lipparini, F.; Egidi, F.; Goings, J.; Peng, B.; Petrone, A.; Henderson, T.; Ranasinghe, D.; Zakrzewski, V. G.; Gao, J.; Rega, N.; Zheng, G.; Liang, W.; Hada, M.; Ehara, M.; Toyota, K.; Fukuda, R.; Hasegawa, J.; Ishida, M.; Nakajima, T.; Honda, Y.; Kitao, O.; Nakai, H.; Vreven, T.; Throssell, K.; Montgomery Jr., J. A.; Peralta, J. E.; Ogliaro, F.; Bearpark, M. J.; Heyd, J. J.; Brothers, E. N.; Kudin, K. N.; Staroverov, V. N.; Keith, T. A.; Kobayashi, R.; Normand, J.; Raghavachari, K.; Rendell, A. P.; Burant, J. C.; Iyengar, S. S.; Tomasi, J.; Cossi, M.; Millam, J. M.; Klene, M.; Adamo, C.; Cammi, R.; Ochterski, J. W.; Martin, R. L.; Morokuma, K.; Farkas, O.; Foresman, J. B.; Fox, D. J. Gaussian 16, Revision C.01. 2016.
(9) Ghosh, A. Electronic Structure of Corrole Derivatives: Insights from Molecular Structures, Spectroscopy, Electrochemistry, and Quantum Chemical Calculations. *Chem. Rev.* 2017, *117* (4), 3798–3881 DOI:10.1021/acs.chemrev.6b00590.
(10) Chai, J.-D.; Head-Gordon, M. Long-range corrected hybrid density functionals with damped atom–atom dispersion corrections. *Phys. Chem. Chem. Phys.* 2008, *10* (44), 6615 DOI:10.1039/b810189b.
(11) Liang, J.; Feng, X.; Hait, D.; Head-Gordon, M. Revisiting the Performance of Time-Dependent Density Functional Theory for Electronic Excitations: Assessment of 43 Popular and Recently Developed Functionals from Rungs One to Four. *J. Chem. Theory Comput.* 2022, *18* (6), 3460–3473 DOI:10.1021/acs.jctc.2c00160.
(12) Concilio, G.; Talotta, C.; Gaeta, C.; Neri, P.; Monaco, G.; Zanasi, R.; Tedesco, D.; Bertucci, C. Absolute Configuration Assignment of Chiral Resorcin[4]arenes from ECD Spectra. *J. Org. Chem.* 2017, *82* (1), 202–210 DOI:10.1021/acs.joc.6b02349.
(13) Petrykowski, W. D.; Vanthuyne, N.; Naim, C.; Bertocchi, F.; Poronik, Y. M.; Ciesielski, A.; Cyrański, M. K.; Terenziani, F.; Jacquemin, D.; Gryko, D. T. Double helicene possessing B–N

dative bonds built on 1,4-dihydropyrrolo[3,2-*b*]pyrrole core. *Chem. Sci.* 2025, *16* (19), 8338–8345 DOI:10.1039/D5SC00540J.
(14) Monaco, G.; Procida, G.; Di Mola, A.; Herrebout, W.; Massa, A. Error bounds on goodness of fit indicators in vibrational circular dichroism spectroscopy. *Chem. Phys. Lett.* 2020, *739*, 137000 DOI:10.1016/j.cplett.2019.137000.
(15) Kubo, H.; Hirose, T.; Nakashima, T.; Kawai, T.; Hasegawa, J.; Matsuda, K. Tuning Transition Electric and Magnetic Dipole Moments: [7]Helicenes Showing Intense Circularly Polarized Luminescence. *J. Phys. Chem. Lett.* 2021, *12* (1), 686–695 DOI:10.1021/acs.jpclett.0c03174.
(16) Furche, F.; Ahlrichs, R.; Wachsmann, C.; Weber, E.; Sobanski, A.; Vögtle, F.; Grimme, S. Circular Dichroism of Helicenes Investigated by Time-Dependent Density Functional Theory. *J. Am. Chem. Soc.* 2000, *122* (8), 1717–1724 DOI:10.1021/ja991960s.